Inorg. Chem. **1993**, *32*, 131–144

Articles

Methane vs Benzene Activation via Transient ${}^t\mathrm{Bu_3SiNHTa({=}NSi{}^tBu_3)_2}$: Structure of $\mathrm{(py)_2MeTa({=}NSi{}^tBu_3)_2}$

Christopher P. Schaller and Peter T. Wolczanski*

Department of Chemistry, Baker Laboratory, Cornell University, Ithaca, New York 14853

Received June 1, 1992

Addition of $\mathrm{Me_3TaCl_2}$ to 2.0 equiv of $\mathrm{LiNHSi{}^tBu_3}$ in hexanes resulted in $\mathrm{CH_4}$ and $({}^t\mathrm{Bu_3SiNH})\mathrm{Me_2Ta{=}NSi{}^tBu_3}$ (**1**, 63%). Thermolysis of **1** in benzene resulted in disproportionation, but in pyridine and THF, $\mathrm{L_2MeTa({=}NSi{}^tBu_3)_2}$ (L = py, **2**(py)$_2$, 68%; THF, **2**(THF)$_2$, 13%) and MeH were produced. The bis adduct **2**(py)$_2$ is considered to form via 1,2-MeH-elimination from $({}^t\mathrm{Bu_3SiNH})\mathrm{Me_2(py)Ta{=}NSi{}^tBu_3}$ (**1**-py), which is obtained from **1** and pyridine at 25 °C. ^{1}H and ^{13}C{^{1}H} NMR spectra of **2**(py)$_2$ manifested equivalent pyridines, but an X-ray structure determination revealed a trigonal bipyramidal, pseudo-C_s stereoisomer with an axial methyl group and equatorial imides that reflects the steric requirements of the bulky ${}^t\mathrm{Bu_3SiN}$ units: orthorhombic, $P2_12_12_1$, $a = 12.134$ (2) Å, $b = 13.421$ (2) Å, $c = 24.865$ (4) Å, $Z = 4$, $V = 4049.3$ (11) Å^3, $T = 295$ K, $R = 6.20\%$, $R_w = 6.64\%$, and GOF = 1.35 for 3257 (88.9%) reflections with ($|F_o| > 3\sigma|F_o|$). Rather long Ta=N bond distances (1.810 (13) and 1.819 (13) Å) support electronic arguments suggesting the imides donate a maximum of 6 electrons to the metal center. Addition of $\mathrm{TaCl_5}$ to 4.0 equiv of $\mathrm{LiNHSi{}^tBu_3}$ in $\mathrm{Et_2O}$ at −78 °C afforded $({}^t\mathrm{Bu_3SiNH})_2\mathrm{ClTa{=}NSi{}^tBu_3}$ (**3**-Cl) and ${}^t\mathrm{Bu_3SiNH_2}$. Alkylation of **3**-Cl with $\mathrm{AlMe_3}$ (hexanes), PhLi ($\mathrm{Et_2O}$/hexanes), $\mathrm{PhCH_2K}$ (toluene), and ${}^t\mathrm{BuCH_2Li}$ ($\mathrm{Et_2O}$) provided $({}^t\mathrm{Bu_3SiNH})_2\mathrm{RTa{=}NSi{}^tBu_3}$ (R = Me, **3**-Me, 78%; Ph, **3**-Ph, 64%; $\mathrm{CH_2Ph}$, **3**-$\mathrm{CH_2Ph}$, 51%; $\mathrm{CH_2{}^tBu}$, **3**-$\mathrm{CH_2{}^tBu}$, 39%). Addition of ${}^t\mathrm{Bu_3SiNH_2}$ or ${}^t\mathrm{Bu_3SiOH}$ to **1** yielded **3**-Me or $({}^t\mathrm{Bu_3SiNH})({}^t\mathrm{Bu_3SiO})\mathrm{MeTa{=}NSi{}^tBu_3}$ (**5**-Me, 52%) and $\mathrm{CH_4}$. Thermolysis of **3**-R effected 1,2-RH-elimination to form transient $({}^t\mathrm{Bu_3SiNH})\mathrm{Ta({=}NSi{}^tBu_3)_2}$ (**4**), a species capable of adding C–H bonds across one imido linkage. Moderate rates of elimination from **3**-R could be obtained only at 182.8 (4) °C: $k_{\mathrm{MeH}} = 8.0\ (1) \times 10^{-6}\ \mathrm{s^{-1}}$, $\Delta G^{\ddagger} = 37.7$ kcal/mol, $k_{\mathrm{MeH}}/k_{\mathrm{MeD}} \geq 3.4$; $k_{\mathrm{PhH}} = 1.67\ (4) \times 10^{-4}\ \mathrm{s^{-1}}$, $\Delta G^{\ddagger} = 35.0$ kcal/mol; $k_{\mathrm{BzH}} = 1.71\ (5) \times 10^{-6}\ \mathrm{s^{-1}}$, $\Delta G^{\ddagger} = 39.1$ kcal/mol. Ground-state information was obtained via the approach to equilibrium of **3**-Ph and $\mathrm{CH_4}$, but observation of a *para*-ditantalum phenyl derivative, $[({}^t\mathrm{Bu_3SiNH})_2\mathrm{Ta{=}NSi{}^tBu_3}]_2(\mu_2{:}\eta^1,\eta^1\text{-}1,4\text{-}\mathrm{C_6H_4})$ ((**3**)$_2\mathrm{C_6H_4}$) complicated the measurement. Simulation of the approach to equilibrium yielded rate constants consistent with the previously measured 1,2-RH-elimination rates and showed that **3**-Me, **3**-Ph, and (**3**)$_2\mathrm{C_6H_4}$ possess relatively similar ground-state free energies. Equilibration of **3**-$\mathrm{CH_2Ph}$ to aryl complexes $({}^t\mathrm{Bu_3SiNH})_2(\mathrm{C_6H_4Me})\mathrm{Ta{=}NSi{}^tBu_3}$ (**3**-$\mathrm{C_6H_4Me}$) in toluene at 182.8 (4) °C gave similar results. The data portray differing 1,2-RH-elimination rates that result from significant transition state energy differences, ruling out a late transition state despite a rough correlation of rate with the C–H bond strength of the eliminated alkane/arene. The implications of these measurements, including the possibility of d^0 alkane or arene complexes as intermediates and differences in tantalum–carbon bond strengths, are discussed in detail.

Introduction

Several apparently disparate systems that activate alkane carbon–hydrogen bonds[1,2] involve a critical, initial electrophilic attack by the metal center. For example, compare the extremely electropositive early transition metal,[3-7] lanthanide,[7-9] and actinide[10] centers (cf. $\mathrm{Cp^*{}_2ScR}$,[7] $\mathrm{Cp^*{}_2LuCH_3}$[8]) that utilize σ-bond metathesis pathways to the softer late transition metal complexes[11-23] (e.g., $\mathrm{Cp^*ML}$, M = Rh, Ir; L = $\mathrm{PR_3}$, CO, etc.[13-15]) that exhibit oxidative addition chemistry. In both instances, the

---

(1) (a) Hill, C., Ed. *Activation and Functionalization of Alkanes*; John Wiley & Sons: New York, 1989. (b) Watson, P. L., Ed. *Selective Hydrocarbon Activation*; VCH Publishers: Toledo, OH, 1989. (c) Shilov, A. E. *Activation of Saturated Hydrocarbons by Transition Metal Complexes*; Reidel: Boston, MA, 1984.

(2) (a) Crabtree, R. H. *Chem. Rev.* **1985**, *85*, 245–269. (b) Bergman, R. G. *Science* **1984**, *223*, 902–908. (c) Graham, W. A. G. *J. Organomet. Chem.* **1986**, *300*, 81–91. (d) Green, M. L. H.; O'Hare, D. *Pure Appl. Chem.* **1985**, *57*, 1897–1910. (e) Halpern, J. *Inorg. Chim. Acta* **1985**, *100*, 41–48. (f) Muetterties, E. L. *Chem. Soc. Rev.* **1983**, *11*, 283–320. (g) Crabtree, R. H.; Hamilton, D. G. *Adv. Organomet. Chem.* **1988**, *28*, 299–338.

(3) Cummins, C. C.; Baxter, S. M.; Wolczanski, P. T. *J. Am. Chem. Soc.* **1988**, *110*, 8731–8733. Details of the zirconium C–H activation chemistry will be published in due course: Cummins, C. C.; Schaller, C. P.; Wolczanski, P. T. Manuscript in preparation.

(4) Cummins, C. C.; Schaller, C. P.; Van Duyne, G. D.; Wolczanski, P. T.; Chan, E. A.-W.; Hoffmann, R. *J. Am. Chem. Soc.* **1991**, *113*, 2985–2994.

(5) (a) Walsh, P. J.; Hollander, F. J.; Bergman, R. G. *J. Am. Chem. Soc.* **1988**, *110*, 8729–8731. (b) Walsh, P. J.; Baranger, A. M.; Bergman, R. G. *Ibid.* **1992**, *114*, 1708–1719.

(6) (a) Jordan, R. F.; Guram, A. S. *Organometallics* **1990**, *9*, 2116–2123. (b) Guram, A. S.; Jordan, R. F.; Taylor, D. F. *J. Am. Chem. Soc.* **1991**, *113*, 1833–1835.

(7) (a) Thompson, M. E.; Baxter, S. M.; Bulls, A. R.; Burger, B. J.; Nolan, M. C.; Santarsiero, B. D.; Schaefer, W. P.; Bercaw, J. E. *J. Am. Chem. Soc.* **1987**, *109*, 203–219. (b) Thompson, M. E.; Bercaw, J. E. *Pure Appl. Chem.* **1984**, *56*, 1–11.

(8) (a) Watson, P. J. *J. Am. Chem. Soc.* **1983**, *105*, 6491–6493. (b) Watson, P. L.; Parshall, G. W. *Acc. Chem. Res.* **1985**, *18*, 51–56.

(9) Evans, W. J.; Chamberlain, L. R.; Ulibarri, T. A.; Ziller, J. W. *J. Am. Chem. Soc.* **1988**, *110*, 6423–6432.

(10) (a) Fendrick, C. M.; Marks, T. J. *J. Am. Chem. Soc.* **1986**, *108*, 425–437. (b) Bruno, J. W.; Smith, G. M.; Marks, T. J.; Fair, C. K.; Schultz, A. J.; Williams, J. M. *Ibid.* **1986**, *108*, 40–56.

(11) (a) Burk, M. J.; Crabtree, R. H. *J. Am. Chem. Soc.* **1987**, *109*, 8025–8032. (b) Crabtree, R. H.; Demou, P. C.; Eden, D.; Mihelcic, J. M.; Parnell, C. A.; Quirk, J. M.; Morris, G. E. *Ibid.* **1982**, *104*, 6994–7001. (c) Crabtree, R. H.; Mihelcic, J. M.; Mellea, M. F.; Quirk, J. M. *Ibid.* **1982**, *104*, 107–113. (d) Crabtree, R. H.; Hamilton, D. G. *Adv. Organomet. Chem.* **1988**, *28*, 299–338.

0020-1669/93/1332-0131$04.00/0

capture of a C–H bond by either a hard[3-10,24,25] or soft electrophile[11-23] renders the substrate susceptible to subsequent events.[26-29] Although evidence for alkane binding prior to σ-bond metatheses or related C–H bond activations by hard metal centers has not yet been reported, intramolecular agostic bonds[30-32] manifest the electrophilicity of these species. The intermediacy of alkane complexes prior to C–H bond oxidative addition has been implicated,[14] similar transients have been observed in related alkyl–hydride reductive eliminations,[33-35] and direct spectroscopic detection of alkane bonding has recently been reported.[36-40]

We[3,4] and others[5] have discovered that certain group 4 imido complexes (i.e., $L_nM{=}N{-}R$) are capable of adding alkane[3] and arene[4,5] C–H bonds to provide amido–alkyl/aryl compounds.[41-45] Interestingly, while the literature regarding the generation of early transition metal imido functionalities is quite extent,[46-58] only a limited number of these species attack C–H bonds. It is apparent that the imide must reside on a metal center that is a potent electrophile and that the critical empty molecular orbital

---

(12) (a) Baudry, D.; Ephritikhine, M.; Felkin, H. *J. Chem. Soc., Chem. Commun.* **1980**, 1243–1244. (b) Cameron, C. J.; Felkin, H.; Fillebeen-Khan, T.; Forrow, N. J.; Guittet, E. *Ibid.* **1986**, 801–802. (c) Ephritikhine, M. *New J. Chem.* **1986**, *10*, 9–15.

(13) Janowicz, A. H.; Bergman, R. G. *J. Am. Chem. Soc.* **1983**, *105*, 3929–3939.

(14) (a) Periana, R. A.; Bergman, R. G. *J. Am. Chem. Soc.* **1986**, *108*, 7332–7346. (b) Buchanan, J. M.; Stryker, J. M.; Bergman, R. G. *Ibid.* **1986**, *108*, 1537–1550. (c) Stoutland, P. O.; Bergman, R. G. *Ibid.* **1988**, *110*, 5732–5744.

(15) (a) Jones, W. D.; Feher, F. J. *Acc. Chem. Res.* **1989**, *22*, 91–100. (b) Jones, W. D.; Feher, F. J. *J. Am. Chem. Soc.* **1984**, *106*, 1650–1663.

(16) (a) Ghosh, C. K.; Graham, W. A. G. *J. Am. Chem. Soc.* **1987**, *109*, 4726–4727. (b) Ghosh, C. K.; Rodgers, D. P. S.; Graham, W. A. G. *J. Chem. Soc., Chem. Commun.* **1988**, 1511–1512. (c) Hoyano, J. K.; McMaster, A. D.; Graham, W. A. G. *J. Am. Chem. Soc.* **1983**, *105*, 7190–7191.

(17) Shinomoto, R. S.; Desrosiers, P. J.; Harper, G. P.; Flood, T. C. *J. Am. Chem. Soc.* **1990**, *112*, 704–713.

(18) (a) Gotzig, J.; Werner, R.; Werner, H. *J. Organomet. Chem.* **1985**, *285*, 99–114. (b) Werner, H.; Gotzig, J. *Ibid.* **1985**, *284*, 73–93.

(19) Antberg, M.; Dahlenberg, L. *Angew. Chem., Int. Ed. Engl.* **1986**, *25*, 260–261.

(20) Chetcuti, P. A.; Hawthorne, M. F. *J. Am. Chem. Soc.* **1987**, *109*, 942–943.

(21) Baker, M. V.; Field, L. D. *J. Am. Chem. Soc.* **1987**, *109*, 2825–2826.

(22) Hackett, M.; Whitesides, G. M. *J. Am. Chem. Soc.* **1988**, *110*, 1449–1462.

(23) (a) Boese, W. T.; Goldman, A. S. *J. Am. Chem. Soc.* **1992**, *114*, 350–351. (b) Maquire, J. A.; Goldman, A. S. *Ibid.* **1991**, *113*, 6706–6708. (c) Sakakura, T.; Sodeyama, T.; Sasaki, K.; Wada, K.; Tanaka, M. *Ibid.* **1990**, *112*, 7221–7229.

(24) (a) Kao, L.-C.; Hutson, A. C.; Sen, A. *J. Am. Chem. Soc.* **1991**, *113*, 700–701. (b) Sen, A.; Gretz, E.; Oliver, T. F.; Jiang, Z. *New J. Chem.* **1989**, *13*, 755–760. (c) Sen, A. *Acc. Chem. Res.* **1988**, *21*, 421–428.

(25) Labinger, J. A.; Herring, A. M.; Bercaw, J. E. *J. Am. Chem. Soc.* **1990**, *112*, 5628–5629.

(26) For possible exceptions, see: Wayland, B. B.; Ba, S.; Sherry, A. E. *J. Am. Chem. Soc.* **1991**, *113*, 5305–5311. Also see refs 27–29.

(27) For H-atom abstractions by cytochrome P-450, see: (a) Ortiz de Montellano, P. R., Ed. *Cytochrome P-450; Structure, Mechanism, and Biochemistry*; Plenum: New York, 1986. (b) Traylor, T. G.; Hill, K. W.; Fann, W.-P.; Tsuchiya, S.; Dunlap, B. E. *J. Am. Chem. Soc.* **1992**, *114*, 1308–1312 and references therein.

(28) For photochemical R–H activations (H-atom abstractions) by polyoxometalates, see: Renneke, R. F.; Kadkhodayan, M.; Pasquali, M.; Hill, C. L. *J. Am. Chem. Soc.* **1991**, *113*, 8357–8367 and references therein.

(29) For C–H bond activation by Hg*, see: Muedas, C. A.; Ferguson, R. R.; Brown, S. H.; Crabtree, R. H. *J. Am. Chem. Soc.* **1991**, *113*, 2233–2242.

(30) (a) Brookhart, M.; Green, M. L. H. *J. Organomet. Chem.* **1983**, *250*, 395–408. (b) Brookhart, M.; Green, M. L. H.; Wong, L. *Prog. Inorg. Chem.* **1988**, *36*, 1–124.

(31) Jordan, R. F.; Bradley, P. K.; Baenziger, N. C.; LaPointe, R. E. *J. Am. Chem. Soc.* **1990**, *112*, 1289–1291 and references therein.

(32) (a) Piers, W. E.; Shapiro, P. J.; Bunel, E. E.; Bercaw, J. E. *Synlett* **1990**, 74–84. (b) den Haan, K. H.; Wielstra, Y.; Teuben, J. H. *Organometallics* **1987**, *6*, 2053–2060. (c) Jeske, G.; Lauke, H.; Mauermann, H.; Swepston, P. N.; Schumann, H.; Marks, T. J. *J. Am. Chem. Soc.* **1985**, *107*, 8091–8103.

(33) Parkin, G.; Bercaw, J. E. *Organometallics* **1989**, *8*, 1172–1179.

(34) Gould, G. L.; Heinekey, D. M. *J. Am. Chem. Soc.* **1989**, *111*, 5502–5504.

(35) Bullock, R. M.; Headford, C. E. L.; Kegley, S. E.; Norton, J. R. *J. Am. Chem. Soc.* **1985**, *107*, 727–729.

(36) (a) Wasserman, E. P.; Moore, C. B.; Bergman, R. G. *Science* **1992**, *255*, 315–318. (b) Weiller, B. H.; Wasserman, E. P.; Bergman, R. G.; Moore, C. B.; Pimentel, G. C. *J. Am. Chem. Soc.* **1989**, *111*, 8288–8290 and references therein.

(37) For short-lived metal–alkane bonds in solution, see: (a) Xie, X.; Simon, J. D. *J. Am. Chem. Soc.* **1990**, *112*, 1130–1136. (b) Wang, L.; Zhu, X.; Spears, K. G. *Ibid.* **1988**, *110*, 8695–8696. (c) Yang, G. K.; Peters, K. S.; Vaida, V. *Chem. Phys. Lett.* **1986**, *125*, 566–568. (d) Klassen, J. K.; Selke, M.; Sorensen, A. A.; Yang, G. K. *J. Am. Chem. Soc.* **1990**, *112*, 1267–1268. (e) For $(OC)_5Cr(H\text{-}SiR_3)$, see: Zhang, S.; Dobson, G. R.; Brown, T. L. *J. Am. Chem. Soc.* **1991**, *113*, 6908–6916.

(38) (a) Perutz, R. N. *Pure Appl. Chem.* **1990**, *62*, 1103–1106. (b) Kafafi, Z. H.; Hauge, R. H.; Margrave, J. L. *J. Am. Chem. Soc.* **1985**, *107*, 6134–6135 and references therein.

(39) For examples of gas-phase alkane complexes, see: Brown, C. E.; Ishikawa, Y.; Hackett, P. A.; Rayner, D. M. *J. Am. Chem. Soc.* **1990**, *112*, 2530–2536 and references therein.

(40) A methane complex precedes activation by FeO^+: Schröder, D.; Fiedler, A.; Hrusák, J.; Schwartz, H. *J. Am. Chem. Soc.* **1992**, *114*, 1215–1222.

(41) For related imido chemistry, see: Doxsee, K. M.; Farahi, J. B.; Hope, H. *J. Am. Chem. Soc.* **1991**, *113*, 8889–8898.

(42) For related group 4 oxo, sulfido, and hydrazido chemistry, see: (a) Carney, M. J.; Walsh, P. J.; Hollander, F. J.; Bergman, R. G. *Organometallics* **1992**, *11*, 761–777. (b) Carney, M. J.; Walsh, P. J.; Hollander, F. J.; Bergman, R. G. *J. Am. Chem. Soc.* **1989**, *111*, 8751–8753. (c) Carney, M. J.; Walsh, P. J.; Hollander, F. J.; Bergman, R. G. *Ibid.* **1990**, *112*, 6426–6428. (d) Walsh, P. J.; Carney, M. J.; Bergman, R. G. *Ibid.* **1991**, *113*, 6343–6345.

(43) For related 1,2-elimination/addition chemistry, see: (a) Parkin, G.; Bercaw, J. E. *Polyhedron* **1988**, *7*, 2053–2082. (b) Parkin, G.; Bercaw, J. E. *J. Am. Chem. Soc.* **1989**, *111*, 391–393. (c) Koelliker, R.; Milstein, D. *Ibid.* **1991**, *113*, 8524–8525.

(44) For related oxo chemisty, see: (a) Herrmann, W. A.; Herdtweck, E.; Floel, M.; Kulpe, J.; Kusthardt, U.; Okuda, J. *Polyhedron* **1987**, *6*, 1165–1182. (b) Rau, M. S.; Kretz, C. M.; Mercando, L. A.; Geoffroy, G. L.; Rheingold, A. L. *J. Am. Chem. Soc.* **1991**, *113*, 7420–7421. (c) Plato, R. S.; Housmekerides, C. E.; Jernakoff, P.; Rubin, D.; Geoffroy, G. L.; Rheingold, A. L. *Organometallics* **1990**, *9*, 2333–2341.

(45) For $M{=}NPh$ functioning as nitrene transfer agent to give $M{\leftarrow}NPh(H)(R)$, see: (a) Lee, S. W.; Trogler, W. C. *Inorg. Chem.* **1990**, *29*, 1659–1662. (b) Gross, M. E.; Johnson, C. E.; Maroney, M. J.; Trogler, W. C. *Ibid.* **1984**, *23*, 2968–2976. (c) Gross, M. E.; Trogler, W. C. *J. Organomet. Chem.* **1981**, *209*, 407–414. (d) Barener, C. J.; Collins, T. J.; Mapes, B. E.; Santarsiero, B. D. *Inorg. Chem.* **1986**, *25*, 4323–4325.

(46) Nugent, W. A.; Mayer, J. M. *Metal-Ligand Multiple Bonds*; Wiley-Interscience: New York, 1988. For recent pertinent studies see refs 46–55 and citations therein.

(47) (a) Chisholm, M. H.; Rothwell, I. P. in *Comprehensive Coordination Chemistry*; Pergamon Press: New York, 1987, Vol. 2, Chapter 13.4. (b) Nugent, W. A.; Haymore, B. L. *Coord. Chem. Rev.* **1980**, *31*, 123–175. (c) Harlan, E. W.; Holm, R. H. *J. Am. Chem. Soc.* **1990**, *112*, 186–193. (d) Holm, R. H. *Chem. Rev.* **1987**, *87*, 1401–1449.

(48) (a) de With, J.; Horton, A. D.; Orpen, A. G. *Organometallics* **1990**, *9*, 2207–2209. (b) C—H activation by a $V{=}NSi^tBu_3$ fragment has been observed in this system. de With, J.; Horton, A. D.; Orpen, A. G. *Abstracts of Papers*; 204th National Meeting of the American Chemical Society; American Chemical Society: Washington, DC, 1992.

(49) Chao, Y.-W.; Wexler, P. A.; Wigley, D. E. *Inorg. Chem.* **1990**, *29*, 4592–4594.

(50) (a) Schrock, R. R.; Crowe, W. E.; Bazan, G. C.; DiMare, M.; O'Regan, M. B.; Schofield, M. H. *Organometallics* **1991**, *10*, 1832–1843. (b) Lichtenhan, J. D.; Critchlow, S. C.; Doherty, N. M. *Inorg. Chem.* **1990**, *29*, 439–442 and references therein.

(51) Parkin, G.; van Asselt, A.; Leahy, D. J.; Whinnery, L.; Hua, N. G.; Quan, R. W.; Henling, L. M.; Schaefer, W. P.; Santarsiero, B. D.; Bercaw, J. E. *Inorg. Chem.* **1992**, *31*, 82–85.

(52) (a) Du, Y.; Rheihgold, A. L.; Maatta, E. A. *J. Am. Chem. Soc.* **1992**, *114*, 345–346. (b) Maatta, E. A.; Du, Y.; Rheingold, A. L. *J. Chem. Soc., Chem. Commun.* **1990**, 756–757. (c) Maatta, E. A.; Du, Y.; *J. Am. Chem. Soc.* **1988**, *110*, 8249–8250.

(53) Chao, Y.-W.; Rodgers, P. M.; Wigley, D. E.; Alexander, S. J.; Rheingold, A. L. *J. Am. Chem. Soc.* **1991**, *113*, 6326–6328.

(54) Williams, D. S.; Schofield, M. H.; Anhaus, J. T.; Schrock, R. R. *J. Am. Chem. Soc.* **1990**, *112*, 6728–6729.

(55) (a) Bazan, G. C.; Oskam, J. H.; Cho, H.-N.; Park, L. Y.; Schrock, R. R. *J. Am. Chem. Soc.* **1991**, *113*, 6899–6907. (b) Schrock, R. R.; Murdzek, J. S.; Bazan, G. C.; Robbins, J.; DiMare, M.; O'Regan, M. *Ibid.* **1990**, *112*, 3875–3886 and references therein.

(56) (a) Hill, J. E.; Fanwick, P. E.; Rothwell, I. P. *Inorg. Chem.* **1991**, *30*, 1143–1144. (b) Hill, J. E.; Profilet, R. D.; Fanwick, P. E.; Rothwell, I. P. *Angew. Chem.* **1990**, *102*, 713–715. See also: (c) Hill, J. E.; Fanwick, P. E.; Rothwell, I. P. *Inorg. Chem.* **1989**, *28*, 3602–3606.

(57) (a) Duchateau, R.; Williams, A. J.; Gambarotta, S.; Chiang, M. Y. *Inorg. Chem.* **1991**, *30*, 4863–4866. (b) Roesky, H. W.; Voelker, H.; Witt, M.; Noltemeyer, M. *Angew. Chem.* **1990**, *102*, 712–713.

(58) Winter, C. H.; Sheridan, P. H.; Lewkebandara, T. S.; Heeg, M. J.; Proscia, J. W. *J. Am. Chem. Soc.* **1992**, *114*, 1095–1097.

Table I. ^{1}H and ^{13}C{^{1}H} NMR Data for Tantalum Imide Complexes in Benzene-d_6

	^{1}H (δ, mult, J (Hz))[a]				^{13}C{^{1}H} (δ)[b]		
compound	$^t\mathrm{Bu_3Si(NH,N)}$[c]	HN	L	other	$^t\mathrm{Bu_3Si(NH,N)}$[d]	L	other
$(^t\mathrm{Bu_3SiNH})\mathrm{Me_2Ta{=}NSi^tBu_3}$ (**1**)	1.13 1.35	6.01		0.77 (Me)	30.16, 23.00 30.83, 24.50		53.51 (Me)
$(^t\mathrm{Bu_3SiNH})\mathrm{Me_2(py)Ta{=}NSi^tBu_3}$ (**1-Py**)	1.26 1.42	6.11	6.50 (m) 6.73 (m) 8.67 (m)		30.43, 23.60 31.07, 24.92	123.96 136.08 150.07	47.13 (Me)
$\mathrm{py_2MeTa({=}NSi^tBu_3)_2}$ (**2**(py)$_2$)	1.51		6.32 (m) 6.58 (m)	0.80 (Me)	31.72, 25.37	124.16 138.19 152.21	37.44 (Me)
$\mathrm{THF_2MeTa({=}NSi^tBu_3)_2}$ (**2**(THF)$_2$)	1.45		1.18 (m) 3.64 (m)	1.01 (Me)	31.35, 25.43	24.70 75.77	33.50 (Me)
$(^t\mathrm{Bu_3SiNH})_2\mathrm{ClTa{=}NSi^tBu_3}$ (**3-Cl**)	1.22 1.37	5.53			30.85, 23.49 31.42, 24.78		
$(^t\mathrm{Bu_3SiNH})_2\mathrm{MeTa{=}NSi^tBu_3}$ (**3-Me**)	1.21 1.38	4.96		0.98 (Me)	30.78, 23.30 31.42, 24.62		30.20 (Me)
$(^t\mathrm{Bu_3SiNH})_2\mathrm{PhTa{=}NSi^tBu_3}$ (**3-Ph**)	1.25 1.36	5.45		7.07 (m) 7.30 (t, 7.5) 8.28 (dd, 1.3, 7.5)	30.84, 23.40 31.41, 24.72		127.89 (Ph para) 128.73 (meta) 141.31 (ortho) 187.82 (ipso)
$(^t\mathrm{Bu_3SiNH})_2(\mathrm{PhCH_2})\mathrm{Ta{=}NSi^tBu_3}$ (**3-CH$_2$Ph**)[e]	1.17 1.36	5.06		3.10 (CH$_2$) 6.85–7.28 (m)	30.80, 23.21 31.44, 24.67		61.50 (CH$_2$) 123.49 (Ph para) 128.56 (meta) 128.99 (ortho) 147.01 (ipso)
$(^t\mathrm{Bu_3SiNH})_2(^t\mathrm{BuCH_2})\mathrm{Ta{=}NSi^tBu_3}$ (**3-CH$_2$^{t}Bu**)	1.27 1.34	4.83		1.34 (Me$_3$) 2.05 (CH$_2$)	30.93, 23.52 31.57, 24.77		34.81 (*C*Me$_3$) 35.69 (Me$_3$) 76.72 (CH$_2$)
$(^t\mathrm{Bu_3SiNH})(^t\mathrm{Bu_3SiO})\mathrm{MeTa{=}NSi^tBu_3}$ (**5-Me**)	1.24 1.37	6.20		1.12 (Me) 1.17 (silox)	30.75, 23.55[f] 30.53, 23.21[f] 31.37, 24.54		34.95 (Me)

[a] Referenced to C$_6$D$_5$H at δ 7.15 or TMS at δ 0.00. [b] Referenced to C$_6$D$_5$H at δ 128.00. [c] The first value corresponds to the amide; the second refers to the imide. [d] The first line refers to the Me and tertiary carbons of the amide; the second refers to the imide. These assignments are tentative. [e] For spectral assignments of the 3-C$_6$H$_4$Me mixture, see the Experimental Section. [f] Corresponds to either the silox or ^{t}Bu$_3$SiNH.

must have some directionality. Transient, three-coordinate $(^t\mathrm{Bu_3SiNH})_2\mathrm{Zr{=}NSi^tBu_3}$[3] and $(^t\mathrm{Bu_3SiNH})\mathrm{XTi{=}NSi^tBu_3}$ (X = halide, NSi^{t}Bu$_3$)[4] species, whose empty $\mathrm{d}_{z^2}/\mathrm{p}_z$ orbitals provide the electrophilic component,[59] and Cp$_2$M═NR derivatives,[5,41,42] which possess a similar empty, directional 2a$_1$ orbital ("d_{y^2}"/p_y),[60] satisfy these constraints and capture C–H bonds. In order to further investigate alkane activations by imido functionalities and test the importance of the initial electrophilic interaction, we initiated a study of related, yet presumably less electrophilic tantalum derivatives, focusing on the generation of $\mathrm{XTa({=}NSi^tBu_3)_2}$. It was hoped that the smaller covalent radius of tantalum (1.34 Å), relative to zirconium (1.45 Å),[61] would permit isolation of the three-coordinate d^0 complex. Instead, important fundamental information pertaining to the activation of methane vs benzene by transient $(^t\mathrm{Bu_3SiNH})\mathrm{Ta({=}N{-}Si^tBu_3)_2}$ was obtained.

Results

Synthesis of Tantalum Imide Complexes. Me$_3$TaCl$_2$[62] proved to be an attractive starting material for the direct synthesis of tantalum amide or imide derivatives. Addition of Me$_3$TaCl$_2$ to 2.0 equiv of LiNHSi^{t}Bu$_3$[63,64] in hexanes resulted in the generation of methane and led to the isolation of colorless, crystalline $(^t\mathrm{Bu_3SiNH})\mathrm{Me_2Ta{=}NSi^tBu_3}$ (**1**) in 63% yield (eq 1). ^{1}H and ^{13}C {^{1}H} NMR (Table I) revealed equivalent tantalum–methyl

$$\mathrm{Me_3TaCl_2 + 2LiNHSi^tBu_3} \xrightarrow[25\,^\circ\mathrm{C},\ -2\mathrm{LiCl}]{\text{hexanes}} \underset{\mathbf{1}}{(^t\mathrm{Bu_3SiNH})\mathrm{Me_2Ta{=}NSi^tBu_3}} + \mathrm{CH_4} \tag{1}$$

groups and two different ^{t}Bu$_3$Si fragments, consistent with a pseudotetrahedral geometry. Amido–imido **1** is related to $(^t\mathrm{Bu_3SiNH})\mathrm{Cl_2V{=}NSi^tBu_3}$ and other complexes prepared by Horton[48] via LiNHSi^{t}Bu$_3$ treatment of VOCl$_3$. Note that **1** contains a maximum of 14 valence electrons, yet neither C–H addition across the imido functionality nor σ-bond metathesis reactivity was observed, as expected from precedent.[46–58] Although the metal center is unsaturated, the electrophilicity is not directional, thereby detering carbon–hydrogen bond-breaking events.

Thermolysis of $(^t\mathrm{Bu_3SiNH})\mathrm{Me_2Ta{=}NSi^tBu_3}$ (**1**) was expected to generate methane and pseudo-trigonal $\mathrm{MeTa({=}NSi^tBu_3)_2}$ (**2**), a transient capable of adding a C—H bond. When heated at 110 °C in C$_6$D$_6$ for 3–4 d, **1** disproportionated to provide several unidentified products and $(^t\mathrm{Bu_3SiNH})_2\mathrm{MeTa{=}NSi^tBu_3}$ (**3-Me**, 40–50% yield), according to ^{1}H NMR spectra (eq 2). Free amine

$$\underset{\mathbf{1}}{(^t\mathrm{Bu_3SiNH})\mathrm{Me_2Ta{=}NSi^tBu_3}} \xrightarrow[110\,^\circ\mathrm{C},\ 3\text{–}4\ \mathrm{d}]{\mathrm{C_6D_6}} \underset{\mathbf{3\text{-}Me}}{(^t\mathrm{Bu_3SiNH})_2\mathrm{MeTa{=}NSi^tBu_3}} + \ldots \tag{2}$$

is likely to play a role in the formation of **3-Me**, since the complex and concomitant methane are rapidly generated (<5 min) upon addition of ^{t}Bu$_3$SiNH$_2$ to **1**, as indicated in eq 3. A 2:1 ratio of

$$\underset{\mathbf{1}}{(^t\mathrm{Bu_3SiNH})\mathrm{Me_2Ta{=}NSi^tBu_3}} + {}^t\mathrm{Bu_3SiNH_2} \xrightarrow[25\,^\circ\mathrm{C}]{\text{benzene}} \underset{\mathbf{3\text{-}Me}}{(^t\mathrm{Bu_3SiNH})_2\mathrm{MeTa{=}NSi^tBu_3}} + \mathrm{CH_4} \tag{3}$$

---

(59) For discussions of related d^1 and d^2 three-coordinate complexes, see: (a) Covert, K. J.; Neithamer, D. R.; Zonnevylle, M. C.; LaPointe, R. E.; Schaller, C. P.; Wolczanski, P. T. *Inorg. Chem.* **1991**, *30*, 2494–2508. (b) Eppley, D. F.; Wolczanski, P. T.; Van Duyne, G. D. *Angew. Chem., Int. Ed. Engl.* **1991**, *30*, 584–585. (c) Covert, K. J.; Wolczanski, P. T.; Hill, S. A.; Krusic, P. J. *Inorg. Chem.* **1992**, *31*, 66–78.

(60) Lauher, J. W.; Hoffman, R. *J. Am. Chem. Soc.* **1976**, *98*, 1729.

(61) Pauling, L. *The Nature of the Chemical Bond*, 3rd ed.; Cornell University Press: Ithaca, NY, 1960.

(62) Schrock, R. R.; Sharp, P. R. *J. Am. Chem. Soc.* **1978**, *100*, 2389–2399.

(63) For the synthesis of ^{t}Bu$_3$SiNH$_2$, see: Nowakowski, P. M.; Sommer, L. H. *J. Organomet. Chem.* **1979**, *178*, 95–103.

(64) Cummins, C. C.; Van Duyne, G. D.; Schaller, C. P.; Wolczanski, P. T. *Organometallics* **1990**, *10*, 164–170.

^{t}Bu$_3$Si resonances and distinct tantalum methyl signals in ^{1}H (δ 0.98, C_6D_6) and $^{13}C\{^1H\}$ NMR (δ 31.30) spectra characterized the pseudotetrahedral molecule. Synthesis and isolation of **3**-Me was most conveniently achieved through metathesis of the corresponding chloride (vide infra).

Donor solvents were utilized to trap the putative bis(imido-methyl) core (**2**) upon thermolysis of (^{t}Bu$_3$SiNH)Me$_2$Ta=NSi^{t}Bu$_3$ (**1**). When heated for 20 h in pyridine at 95 °C for 20 h, **1** released 1.0 equiv of MeH, according to Toepler pump measurements, and (py)$_2$MeTa(=NSi^{t}Bu$_3$)$_2$ (**2**(py)$_2$, >90% yield by ^{1}H NMR) was generated as shown in eq 4. Upon scaleup, **2**(py)$_2$ was isolated as amber crystals in 68% yield. A similar thermolysis of **1** in THF at 105 °C for 68 h proved less satisfactory. Only 0.56 equiv of MeH were released (Toepler) and an oily yellow-brown residue remained after removal of the THF. Fortunately, off-white crystals of (THF)$_2$MeTa(=NSi^{t}Bu$_3$)$_2$ (**2**-THF$_2$) were obtained upon crystallization from hexanes, although the yield was low (13%). For both adducts **2**(L)$_2$, room-temperature ^{1}H and $^{13}C\{^1H\}$ NMR data suggested that the dative ligands occupied equivalent positions; thus a trigonal bipyramidal configuration was considered most likely, with the bulky ^{t}Bu$_3$SiN imido π-donors residing in equatorial sites.[65] An X-ray structural investigation of **2**(py)$_2$ revealed the expected distorted tbp geometry, but the py ligands occupy both axial and equatorial positions (vide infra).

$$\underset{\mathbf{1}}{(^t\mathrm{Bu_3SiNH})\mathrm{Me_2Ta{=}NSi^tBu_3}} \xrightarrow[\sim 100\ ^\circ\mathrm{C}]{\text{py or THF}} \mathrm{L_2MeTa({=}NSi^tBu_3)_2} + \mathrm{MeH} \quad (4)$$

$$\mathrm{L} = \mathrm{py},\ \mathbf{2}(\mathrm{py})_2;\ \mathrm{THF},\ \mathbf{2}(\mathrm{THF})_2$$

Bis adducts L$_2$MeTa(=NSi^{t}Bu$_3$)$_2$ (**2**(L)$_2$) could be considered to form via 1,2-elimination of MeH from (^{t}Bu$_3$SiNH)-Me$_2$Ta=NSi^{t}Bu$_3$ (**1**) to yield MeTa(=NSi^{t}Bu$_3$)$_2$ (**2**), followed by trapping with 2 equiv of L. Alternatively, L may form an adduct with **1**, and 1,2-elimination of MeH would then occur via (^{t}Bu$_3$SiNH)Me$_2$LTa=NSi^{t}Bu$_3$ (**1**-L) to give methane and LMeTa(=NSi^{t}Bu$_3$)$_2$ (**2**-L) which is trapped by another L. Support for the latter possibility was evidenced when (^{t}Bu$_3$SiNH)Me$_2$(py)Ta=NSi^{t}Bu$_3$ (**1**-py) formed upon exposure of **1** to pyridine at 25 °C (eq 5), followed by solvent removal and precipitation from hexanes. In ^{1}H and $^{13}C\{^1H\}$ NMR spectra of **1**-py, a single resonance for the TaMe$_2$ group was accompanied by signals attributed to two distinct ^{t}Bu$_3$Si fragments. Given the ready formation of **1**-py, it is likely that the presumed rate-determining step in the formation of (py)$_2$MeTa(=NSi^{t}Bu$_3$)$_2$ (**2**(py)$_2$), the 1,2-elimination of MeH, occurs from five-coordinate **1**-py. This result contrasts with previous eliminations of RH (R = Me, Cy, Ph) and ^{t}Bu$_3$SiNH$_2$ from (^{t}Bu$_3$SiNH)$_3$ZrR[3] and (^{t}Bu$_3$SiNH)$_3$TiX (X = Cl, Br, ^{t}Bu$_3$SiNH),[4] respectively, which occur directly from a four-coordinate ground state. In addition, the demonstrably slower degradation of **1** in benzene-d_6 vs donor solvents contradicts a 1,2-MeH-elimination from the four-coordinate dimethyl species (**1**).

$$\underset{\mathbf{1}}{(^t\mathrm{Bu_3SiNH})\mathrm{Me_2Ta{=}NSi^tBu_3}} \xrightarrow[25\ ^\circ\mathrm{C},\ <5\ \mathrm{min}]{\text{pyridine}} \underset{\mathbf{1}\text{-py}}{(^t\mathrm{Bu_3SiNH})\mathrm{Me_2(py)Ta{=}NSi^tBu_3}} \quad (5)$$

Since the sought-after C–H activation reactivity was not found in the chemistry of (^{t}Bu$_3$SiNH)Me$_2$Ta=NSi^{t}Bu$_3$ (**1**) and its thermolysis products, tantalum derivatives directly related to the aforementioned (^{t}Bu$_3$SiNH)$_3$MX (M = Zr, X = alkyl; M = Ti, X = halide) species were targeted. Addition of TaCl$_5$ to 4.0 equiv of LiNHSi^{t}Bu$_3$ in Et$_2$O at −78 °C and subsequent stirring at 25 °C for 12 h resulted in the formation of (^{t}Bu$_3$SiNH)$_2$-ClTa=NSi^{t}Bu$_3$ (**3**-Cl) and ^{t}Bu$_3$SiNH$_2$ (eq 6).[66] Colorless, crystalline **3**-Cl was isolated from hexanes in 82% yield and possessed a 2:1 ratio of ^{t}Bu$_3$Si groups in ^{1}H and $^{13}C\{^1H\}$ NMR spectra, as expected for a pseudotetrahedral coordination sphere.

$$\mathrm{TaCl_5} + 4\mathrm{LiNHSi^tBu_3} \xrightarrow[-4\mathrm{LiCl}]{\mathrm{Et_2O},\ 25\ ^\circ\mathrm{C}} \underset{\mathbf{3}\text{-Cl}}{(^t\mathrm{Bu_3SiNH})_2\mathrm{ClTa{=}NSi^tBu_3}} + {}^t\mathrm{Bu_3SiNH_2} \quad (6)$$

Initial efforts to alkylate (^{t}Bu$_3$SiNH)$_2$ClTa=NSi^{t}Bu$_3$ (**3**-Cl) proved troublesome. Attempts using MeLi led to some (^{t}Bu$_3$SiNH)$_2$MeTa=NSi^{t}Bu$_3$ (**3**-Me), but some starting material remained and a byproduct, tentatively formulated as Li[(^{t}Bu$_3$SiNH)MeTa(=NSi^{t}Bu$_3$)$_2$] in reference to Horton's crystallographically characterized Li[(^{t}Bu$_3$SiN=)$_2$VMe$_2$],[48] was difficult to avoid. Successful methylation was effected via the addition of 1.0 equiv of AlMe$_3$ (in hexanes) to **3**-Cl in hexanes at −78 °C. Subsequent stirring at 25 °C for ~12 h resulted in the production of **3**-Me (eq 7), which was isolated as colorless crystals from hexanes in 78% yield. Other colorless, crystalline alkyl complexes were straightforwardly prepared in moderate yields from **3**-Cl and various alkyl anion equivalents. Phenyllithium was added to **3**-Cl in Et$_2$O/hexanes to produce (^{t}Bu$_3$SiNH)$_2$PhTa=NSi^{t}Bu$_3$ (**3**-Ph) in 64% yield (eq 8), and a similar addition of PhCH$_2$K to **3**-Cl in toluene afforded (^{t}Bu$_3$SiNH)$_2$(PhCH$_2$)Ta=NSi^{t}Bu$_3$ (**3**-CH$_2$Ph) in 51% yield (eq 9). Excess ^{t}BuCH$_2$Li (~2 equiv) was needed to cleanly provide (^{t}Bu$_3$SiNH)$_2$(^{t}BuCH$_2$)Ta=NSi^{t}Bu$_3$ (**3**-CH$_2{}^t$Cu) from a related metathetical procedure (eq 10), but the yield was somewhat low (39%). In the latter instances, the isolated yields were significantly lower than those observed in NMR tube reactions (~95%) due to the high solubilities of the benzyl (**3**-CH$_2$Ph) and neopentyl (**3**-CH$_2{}^t$Bu) compounds. For each new alkyl derivative, ^{1}H and $^{13}C\{^1H\}$ NMR spectra displayed a 2:1 ratio of amide–imide ^{t}Bu$_3$Si fragments in addition to pertinent Ta–R resonances (Table I). As expected, 1,2-RH-elimination from **3**-R generates three-coordinate (^{t}Bu$_3$SiNH)Ta(=NSi^{t}Bu$_3$)$_2$ (**4**), a species capable of activating carbon-hydrogen bonds (vide infra).

$$\underset{\mathbf{3}\text{-Cl}}{(^t\mathrm{Bu_3SiNH})_2\mathrm{ClTa{=}NSi^tBu_3}} + \mathrm{AlMe_3} \xrightarrow[25\ ^\circ\mathrm{C},\ 12\ \mathrm{h}]{\text{hexanes}} \underset{\mathbf{3}\text{-Me}}{(^t\mathrm{Bu_3SiNH})_2\mathrm{MeTa{=}NSi^tBu_3}} + \mathrm{ClAlMe_2} \quad (7)$$

$$\underset{\mathbf{3}\text{-Cl}}{(^t\mathrm{Bu_3SiNH})_2\mathrm{ClTa{=}NSi^tBu_3}} + \mathrm{PhLi} \xrightarrow[\mathrm{Et_2O/hexanes},\ -\mathrm{LiCl}]{25\ ^\circ\mathrm{C},\ 12\ \mathrm{h}} \underset{\mathbf{3}\text{-Ph}}{(^t\mathrm{Bu_3SiNH})_2\mathrm{PhTa{=}NSi^tBu_3}} \quad (8)$$

$$\mathbf{3}\text{-Cl} + \mathrm{PhCH_2K} \xrightarrow[\text{toluene},\ -\mathrm{KCl}]{25\ ^\circ\mathrm{C},\ 12\ \mathrm{h}} \underset{\mathbf{3}\text{-CH}_2\mathrm{Ph}}{(^t\mathrm{Bu_3SiNH})_2(\mathrm{PhCH_2})\mathrm{Ta{=}NSi^tBu_3}} \quad (9)$$

$$\mathbf{3}\text{-Cl} + {}^t\mathrm{BuCH_2Li} \xrightarrow[\mathrm{Et_2O},\ -\mathrm{LiCl}]{25\ ^\circ\mathrm{C},\ 12\ \mathrm{h}} \underset{\mathbf{3}\text{-CH}_2{}^t\mathrm{Bu}}{(^t\mathrm{Bu_3SiNH})_2(^t\mathrm{BuCH_2})\mathrm{Ta{=}NSi^tBu_3}} \quad (10)$$

---

[65] Rossi, A. R.; Hoffmann, R. *Inorg. Chem.* **1975**, *14*, 365–374.

[66] For the related [(^{t}BuNH)(^{t}BuNH$_2$)ClTa=N^{t}Bu]$_2$(μ-Cl)$_2$, see: Jones, T. C.; Nielson, A. J.; Ricard, C. E. F. *J. Chem. Soc., Chem. Commun.* **1984**, 205–206.

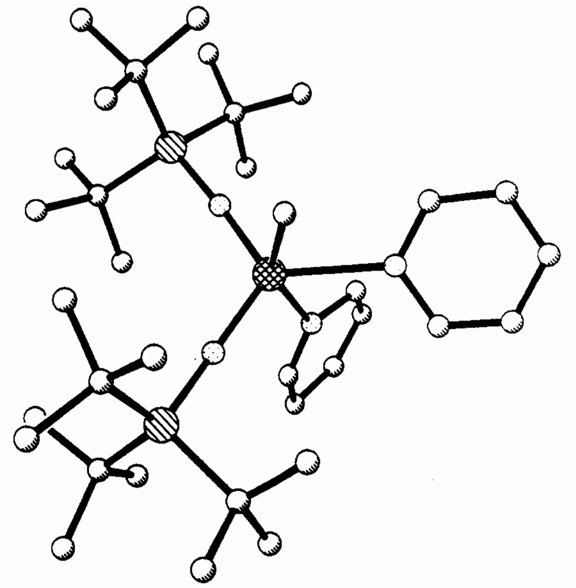

Figure 1. Molecular view of $(py)_2MeTa({=}NSi^tBu_3)_2$ (**2**$(py)_2$).

Table II. Crystallographic Data for $(py)_2MeTa({=}NSi^tBu_3)_2$ (**2**$(py)_2$)

formula: $C_{35}H_{67}N_4Si_2Ta$	fw = 781.1
a = 12.134(2) Å	space group: $P2_12_12_1$
b = 13.421(2) Å	T = 25°C
c = 24.865(4) Å	λ = 0.710 70 Å
ρ_{calc} = 1.281 g	μ = 2.766 mm^{-1}
V = 4049.3(11) Å^3	R = 0.062^a
Z = 4	R_w = 0.066^b

[a] $R = \sum||F_o| - |F_c||/(\sum|F_o|)$. [b] $R_w = \{\sum w(|F_o| - |F_c|)^2/\sum w(|F_o|)^2\}^{1/2}$.

In order to vary the composition of the ancillary ligands, and the electrophilicity at tantalum, $^tBu_3SiO$ was considered as a replacement for $^tBu_3SiNH$. As eq 11 indicates, $(^tBu_3SiNH)Me_2Ta{=}NSi^tBu_3$ (**1**) and 1.0 equiv of $^tBu_3SiOH$ were combined in hexane for ~30 min at 25 °C, yielding CH_4 and $(^tBu_3SiNH)(^tBu_3SiO)MeTa{=}NSi^tBu_3$ (**5**-Me), which was isolated in 52% yield from hexane as colorless crystals.

$$\underset{\mathbf{1}}{(^tBu_3SiNH)Me_2Ta{=}NSi^tBu_3} + {}^tBu_3SiOH \xrightarrow[25\ ^\circ C,\ \sim 30\ min]{hexane} \underset{\mathbf{5\text{-}Me}}{(^tBu_3SiNH)(^tBu_3SiO)MeTa{=}NSi^tBu_3} + CH_4 \quad (11)$$

Molecular Structure of $(py)_2MeTa({=}NSi^tBu_3)_2$ (2$(py)_2$). A single-crystal X-ray structure determination (orthorhombic, $P2_12_12_1$, 3257 reflections ($F > 3.0\sigma(F)$), R = 6.2%, R_w = 6.6%) of $(py)_2MeTa({=}NSi^tBu_3)_2$ (**2**$(py)_2$) confirmed its molecular formula and trigonal bipyramidal geometry, but revealed an unanticipated pseudo-C_s stereoisomer. As the molecular view in Figure 1 illustrates (crystallographic data given in Table II), the methyl group of **2**$(py)_2$ occupies an axial position, in contrast to ^1H and $^{13}C\{^1H\}$ NMR evidence that points to a more symmetric C_{2v} structure with diaxial pyridines. Since the bulky, π-donating $^tBu_3SiN{=}$ ligands are relegated to the least sterically demanding equatorial sites,[65] the pyridines reside in the remaining axial and equatorial positions, although significant distortions from a true tbp framework are observed. Curiously, the configuration of **2**$(py)_2$ is distinct from that of a related bis(arylimido) derivative, $(py)_2ClTa({=}NAr)_2$ (Ar = 2,6-$^iPr_2C_6H_3$), prepared by Wigley et al.,[49] which displays the expected C_{2v} conformation. Electronic arguments suggest that chloride should prefer an equatorial rather than an axial site because the former is marginally better for a π-donor. Similar arguments also suggest that a good σ-donor will occupy an equatorial site in preference to an axial one;[65] hence **2**$(py)_2$ should also be C_{2v} because CH_3^- is a stronger σ-donor than py. The disparity between the two structures is probably due to the more pronounced steric influences of the conical $^tBu_3SiN{=}$ ligands as compared with the more wedgelike shape of the arylimido groups.[67] In the $(py)_2ClTa({=}NAr)_2$ complex, the ring of one arylimido moiety is virtually in the N_2TaCl equatorial plane, while the other is perpendicular to it, thus permitting some steric relief for the axially disposed pyridines, which are rotated to minimize interactions with the latter.

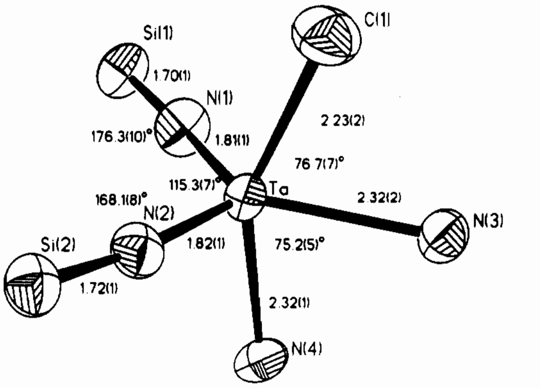

Figure 2. Skeletal view of $(py)_2MeTa({=}NSi^tBu_3)_2$ (**2**$(py)_2$).

Distortions from ideal tbp geometry reflect the steric demands of the silimido ligands (Figure 2, Table III). The axial substituents lean away from the imides as indicated by the C_{ax}–Ta–$N(py)_{eq}$ and $N(py)_{ax}$–Ta–$N(py)_{eq}$ angles of 76.7 (7) and 75.2 (5)°, respectively; the C_{ax}–Ta–$N(py)_{ax}$ angle of 151.9 (7)° is ~10° less than the corresponding angle in $(py)_2ClTa({=}NAr)_2$, corroborating the greater steric influence by the $^tBu_3SiN{=}$ groups. The premise that the deviation from an ideal 180° is due to the presence of the bulky imides is borne out by the nearly equivalent set of $N1_{im}$–Ta–C_{ax} (99.0 (7)°) and $N2_{im}$–Ta–C_{ax} (98.9 (7)°) angles, in addition to similar $N1_{im}$–Ta–py_{ax} (94.0 (6)°) and $N2_{im}$–Ta–C_{ax} (97.8 (5)°) angles. Somewhat surprisingly, the steric influence of the imides is not manifested by the $N1_{im}$–Ta–$N2_{im}$ angle of 115.3(7)°; the analogous angle in $(py)_2ClTa({=}NAr)_2$ is also less than the ideal 120° (113.2 (3)°). The imides and equatorial pyridine ligand are virtually coplanar, as evidenced by the 120.4 (6) and 124.2 (6)° angles pertaining to $N1_{im}$–Ta–py_{eq} and $N2_{im}$–Ta–Py_{eq}, respectively. The deviation of the $N1_{im}$–Ta–$N2_{im}$ angle from the 120° ideal value is attributed to both σ- and π-electronic components of the bonding. First, assuming the imides form better σ-bonds than the pyridine, a closing of the $N1_{im}$–Ta–$N2_{im}$ angle permits better overlap with the $d_{x^2-y^2}/p_x$ and d_{xy}/p_y (aligning z axially) hybrid orbitals. Second, π-donation from the imides into the lower lying d_{xz},d_{yz} orbitals is similarly maximized when $N1_{im}$–Ta–$N2_{im}$ approaches 90°, since py_{eq} is not a competitive π-donor. Third, only the symmetric combination of the two in-plane (equatorial) pπ-orbitals of the $N1_{im}$–Ta–$N2_{im}$ unit is significant, overlapping with the $d_{x^2-y^2}/p_x$ hybrid; this interaction is also maximized as $N1_{im}$–Ta–$N2_{im}$ nears 90°. As a consequence of their disposition, the two imides contribute roughly 6 rather than the maximum 8 e$^-$ to the metal center, not unlike the bonding in certain bis(acetylene) adducts;[68] hence, the complex is probably best considered a 16 e$^-$ species. Related arguments apply to Wigley's $(py)_2ClTa({=}NAr)_2$ compound.[49]

In corroboration with the above contention regarding imido bonding, the Ta=N bond distances (1.810 (13) and 1.819 (13) Å) are somewhat long, especially in comparison to complexes such as $(Me_2N)_3Ta{\equiv}N^tBu$ (1.77 (2) Å)[69] and (Et_3P)-

---

(67) For similar arguments pertaining to alkoxides, see: Lubben, T. V.; Wolczanski, P. T.; Van Duyne, G. D. *Organometallics* **1984**, *3*, 977–983.

(68) (a) Templeton, J. L.; Ward, B. C. *J. Am. Chem. Soc.* **1980**, *102*, 3288–3290. (b) Templeton, J. L. *Adv. Organomet. Chem.* **1989**, *29*, 1–100.

(69) Nugent, W. A.; Harlow, R. L. *J. Chem. Soc., Chem. Commun.* **1978**, 579–580.

Table III. Selected Interatomic Distances (Å) and Angles (deg) for $(py)_2MeTa({=}NSi^tBu_3)_2$ ($\mathbf{2}(py)_2$)[a]

Ta–Cl	2.226 (18)	Ta–N1	1.810 (13)	Ta–N2	1.819 (13)
Ta–N3	2.324 (15)	Ta–N4	2.316 (14)	Si1–N1	1.702 (13)
Si2–N2	1.719 (14)	Si–C	1.93 $(3)_{av}$	C–C (^{t}Bu)	1.53 $(4)_{av}$
C–C (py)	1.35 (4)	N–C (py)	1.31 (6)		
Cl–Ta–N1	99.0 (7)	Cl–Ta–N2	98.9 (7)	Cl–Ta–N3	76.7 (7)
Cl–Ta–N4	151.9 (7)	N1–Ta–N2	115.3 (7)	N1–Ta–N3	120.4 (6)
N1–Ta–N4	94.0 (6)	N2–Ta–N3	124.2 (6)	N2–Ta–N4	97.8 (5)
N3–Ta–N4	75.2 (5)	Ta–N1–Si1	176.3 (10)	Ta–N2–Si2	168.1 (8)
Ta–N–C	122.4 $(9)_{av}$	C–N–C	114.9 $(24)_{av}$	N–C–C	124.9 $(68)_{av}$
C–C–C (py)	118.4 $(35)_{av}$	N–Si–C	107.4 $(19)_{av}$	Si–C–C	112.3 $(23)_{av}$
C–Si–C	111.4 $(17)_{av}$	C–C–C (im)	106.4 $(24)_{av}$		

[a] Differences between the axial and equatorial pyridines are statistically insignificant.

Scheme I

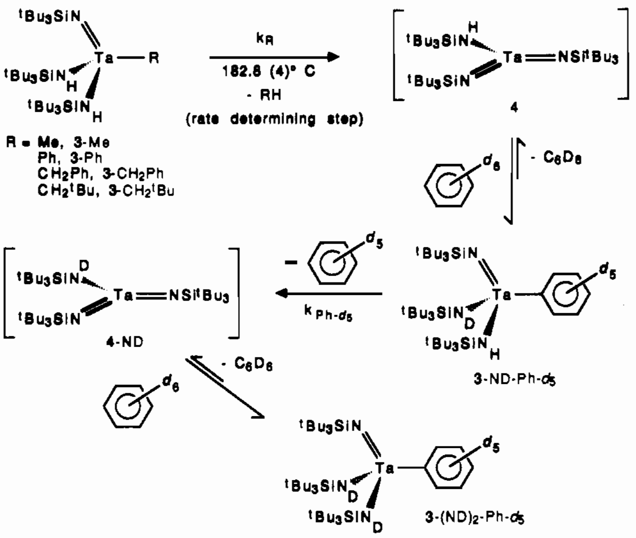

$(THF)Cl_2Ta{\equiv}NPh$ (1.765 (5) Å),[70] where the bond lengths are more consistent with triple bonding. The distances thus place the tantalum–nitrogen bond order between 2 and 3, a conclusion reached previously by Bercaw et al.[51] in assessing the bonding in $Cp^*_2(H)Ta{=}NPh$ (d(Ta=N) = 1.831 (10) Å). Also observed for this recent structure is nearly linear $Ta{=}N{-}C_{ipso}$ angle of 177.8 (9)° that implicates sp hybridization at N, but not necessarily Ta≡N bonding. Although the Ta=N—Si angles in $\mathbf{2}(py)_2$ are 176.3 (10) and 168.1 (8)°, caution must be used in overinterpreting the influence of $N(p\pi)\rightarrow Ta(d\pi)$ donation, as Rothwell[71] has noted for relevant alkoxide complexes. While steric arguments do not support linearity in $\mathbf{2}(py)_2$, $N(p\pi)\rightarrow Si(d\pi)$ bonding may contribute to the straightened alignments. The tantalum–carbon distance of 2.23 (2) Å is unremarkable, as are the virtually equivalent axial and equatorial pyridine–tantalum bonds (2.316 (14) and 2.324 (15) Å, respectively); differences in internal bond distances and angles between the two pyridine ligands are statistically insignificant. Examination of the unit cell suggests that the orientation of the pyridines is dictated by a combination of intramolecular steric and intermolecular packing forces. Similar subtle forces acting on the Si^tBu_3 units help relegate the molecule to its pseudo-C_s, chiral conformation consistent with the $P2_12_12_1$ space group.

1,2-RH-Elimination Studies. The 1,2-elimination of RH from $(^tBu_3SiNH)_2RTa{=}NSi^tBu_3$ (R = Me (**3**-Me), Ph (**3**-Ph), CH_2Ph (**3**-CH_2Ph), $CH_2{}^tBu$ (**3**-$CH_2{}^tBu$)) was monitored via kinetics, and the data are consistent with the overall reaction sequence indicated by Scheme I. Note that the RH loss and C_6D_5H loss steps, k_R and $k(Ph\text{-}d_5)$ respectively, may be considered irreversible because the reaction is conducted in C_6D_6 solvent, which is a competitive trapping agent in high concentration. ^1H NMR spectra (C_6D_6) were used to follow the first-order disappearance manifested by the amido protons of **3**-R over ~5–6 half-lives as $(^tBu_3SiND)_2(C_6D_5)Ta{=}NSi^tBu_3$ (**3**$(ND)_2Ph$-d_5) formed (Table IV). Thermolysis of **3**-CH_3 in C_6D_6 at 182.8 °C produced solely CH_4, thereby implicating 1,2-elimination (k_R) to a three-coordinate intermediate, $(^tBu_3SiNH)Ta({=}NSi^tBu_3)_2$ (**4**), rather than σ-bond metathesis or pathways initiated by amine elimination. The rate of alkane elimination was unaffected by addition of free $^tBu_3SiNH_2$, supporting the latter contention. By measurement of the rate of CH_3D loss from $(^tBu_3SiND)_2(CH_3)Ta{=}NSi^tBu_3$ (**3**$(ND)_2Me$), a k_H/k_D of ≥3.4(3) at 182.8 °C was calculated,[72] consistent with abstraction of the amido proton/deuterium by the methyl group. The substantial kinetic isotope effect, which has precedent in related abstractions,[73,74] may indicate a fairly linear transition state.[75]

An added complication to the overall process concerns the *relatively* rapid addition/elimination of benzene-d_6 to and from the transient bis(imido) species $(^tBu_3SiNH)Ta({=}NSi^tBu_3)_2$ (**4**). Since elimination of R–H from **3**-R (k_R) is slower than C_6D_5H loss ($k(Ph\text{-}d_5)$) from penultimate $(^tBu_3SiNH)(^tBu_3SiND)(C_6D_5)Ta{=}NSi^tBu_3$ (**3**-ND-Ph-d_5), the final phenyl derivative contains fully deuterated amide sites (i.e., $(^tBu_3SiND)_2(C_6D_5)Ta{=}NSi^tBu_3$ (**3**$(ND)_2Ph$-d_5). Previous studies involving thermolysis of $(^tBu_3SiNH)_3ZrR$ in benzene-d_6 revealed a similar occurrence. Where R = Ph, the above supposition is not true, and the first-formed stable intermediate, **3**-ND-Ph-d_5, cannot be distinguished from the starting material (**3**-Ph) by ^1H NMR. In this instance, the reaction was monitored by disappearance of the phenyl ortho hydrogen ($1.67 (4) \times 10^{-4}$ s^{-1}), and by loss of the NH resonance ($1.43 (8) \times 10^{-4}$ s^{-1}). The latter requires taking account of the sequential C_6H_6 (k_R) and C_6D_5H ($k(Ph\text{-}d_5)$) loss steps;[76] the similar rate constants further serve to corroborate the above scheme.

The temperature of 182.8 °C needed to conveniently observe the 1,2-elimination rates ($k_R \sim 10^{-4}$–10^{-6} s^{-1}) testifies to the stability of the $(^tBu_3SiNH)_2RTa{=}NSi^tBu_3$ (**3**-R) derivatives. Unfortunately, the harsh conditions prevent expedient temper-

---

(70) Churchill, M. R.; Wasserman, H. J. *Inorg. Chem.* **1982**, *21*, 223–226.

(71) Steffey, B. D.; Fanwick, P. E.; Rothwell, I. P. *Polyhedron* **1990**, *9*, 963–968.

(72) The thermolysis of $(^tBu_3SiND)_2(CH_3)Ta{=}NSi^tBu_3$ (**3**-$(ND)_2Me$) was slow enough that some decomposition, presumably protolytic, is competitive, as indicated by the presence of CH_4. Consequently, the k_H/k_D of ≥3.4 must be considered a minimum value.

(73) (a) Buchwald, S. L.; Nielsen, R. B. *J. Am. Chem. Soc.* **1988**, *110*, 3171–3175. (b) Mayer, J. M.; Curtis, C. J.; Bercaw, J. E. *Ibid.* **1983**, *105*, 2651–2660. (c) Schock, L. E.; Brock, C. P.; Marks, T. J. *Organometallics* **1987**, *6*, 232–241. (d) McDade, C.; Green, J. C.; Bercaw, J. E. *Ibid.* **1982**, *1*, 1629–1634. (e) Luinstra, G. A.; Teuben, J. H. *Ibid.* **1992**, *11*, 1793–1801.

(74) For similar systems which undergo alternate abstractions, see: (a) Nugent, W. A.; Ovenall, D. W.; Holmes, S. J. *Organometallics* **1983**, *2*, 161–162. (b) Nugent, W. A.; Zubyk, R. M. *Inorg. Chem.* **1986**, *25*, 4604–4606. (c) Takahashi, Y.; Onoyama, N.; Ishikawa, Y.; Motojima, S.; Sugiyama, K. *Chem. Lett.* **1978**, 525–528.

(75) (a) Carpenter, B. K. *Determination of Reaction Mechanisms*; Wiley-Interscience: New York, 1984. (b) Lowry, T. H.; Richardson, K. S. *Mechanism and Theory in Organic Chemistry*, 2nd ed.; Harper and Row: New York, 1981, and references therein.

(76) Frost, A. A.; Pearson, R. G. *Kinetics and Mechanism*; John Wiley and Sons: New York, 1961.

Table IV. Selected Rate Constants[a] for the Elimination of RH from $({}^t\mathrm{Bu_3SiNH})_2\mathrm{RTa{=}NSi^tBu_3}$ in C_6D_6 or C_6D_{12}

$({}^t\mathrm{Bu_3SiNH/D})_2\mathrm{RTa{=}NSi^tBu_3}$	concn (M)	k (10^6 s^{-1}, 182.8 °C)	$\Delta G^{\ddagger}$ (kcal/mol)[b]
R = Me (3-Me)[c]	0.035 (1)	8.0 (1)	37.7
		9.0[d]	37.6[d]
R = Me (3-(ND)$_2$-Me)[c]	0.033 (1)	2.35 (8)	38.8
R = Ph (3-Ph)	0.032 (1)	167 (4)[e]	35.0[e]
	0.032 (1)	143 (8)[f]	35.1[f]
		150[d]	35.1[d]
R = $({}^t\mathrm{Bu_3SiNH}){}^t\mathrm{Bu_3SiNTa}$-($\mu_2{:}\eta^1,\eta^1$-1,4-$C_6H_4$) ((3)$_2C_6H_4$)		400[d]	34.2[d]
R = CH$_2$Ph (3-CH$_2$Ph)	0.031 (1)	1.71 (5)	39.1
R = CH$_2{}^t$Bu (3-CH$_2{}^t$Bu)	0.028 (1)	22.3 (6)	36.8
$({}^t\mathrm{Bu_3SiO})({}^t\mathrm{Bu_3SiNH})\mathrm{Me}$-$\mathrm{TaNSi^tBu_3}$ (5-Me)	0.015 (1)	1.02 (4)	39.6

[a] Determined from weighted, non-linear, least-squares fitting of the differential form of the rate expression. [b] From the error estimates of the rate constants, the error in $\Delta G^{\ddagger}$ is ≤0.1 kcal/mol in each case. [c] Tandem measurement. [d] Determined from Runga–Kutta fit of the approach to equilibrium by 3-Ph and MeH in C_6D_{12}. [e] Determined via disappearance of the phenyl para hydrogen. [f] Determined via disappearance of the amide hydrogens, which occurs in two sequential first-order steps (see text).

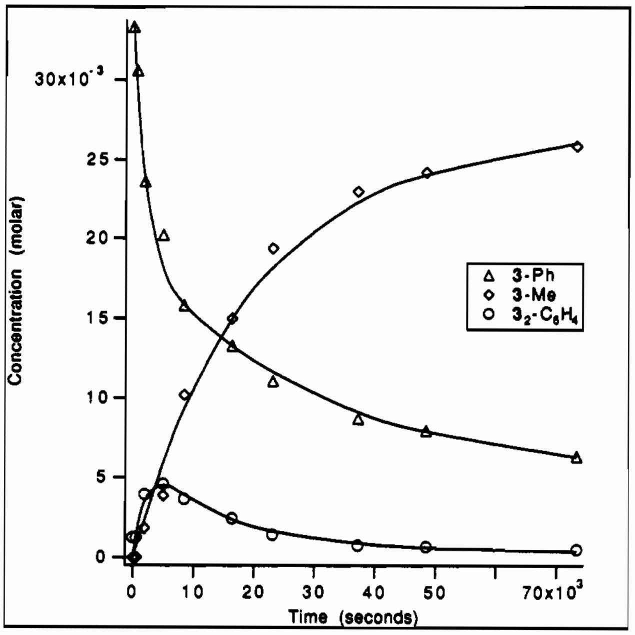

Figure 3. Approach to equilibrium by $({}^t\mathrm{Bu_3SiNH})_2\mathrm{PhTa{=}NSi^tBu_3}$ (3-Ph) and CH_4. The data points were fit by trial and error via a Runge–Kutta simulation: Δ = 3-Ph; ◇ = $({}^t\mathrm{Bu_3SiNH})_2\mathrm{MeTa{=}NSi^tBu_3}$ (3-Me); O = $[({}^t\mathrm{Bu_3SiNH})_2\mathrm{Ta{=}NSi^tBu_3}]_2(\mu_2{:}\eta^1,\eta^1\text{-}1,4\text{-}C_6H_4)$ ((3)$_2$C$_6$H$_4$).

ature-dependent 1,2-elimination studies; hence, the activation parameters for the reaction were not determined, and it is assumed that the process models previous cases. At temperatures >190 °C, other degradation pathways, probably protolytic in origin, hamper accurate kinetic measurements.

A brief glimpse of the rate constants listed in Table IV reveals a few surprises. In comparison to the 1,2-eliminations of RH from $({}^t\mathrm{Bu_3SiNH})_3\mathrm{ZrR}$, the magnitudes of the rate constants are truly dramatic. For example, MeH elimination from 3-Me occurs with $\Delta G^{\ddagger}_{182.8\,°\mathrm{C}} = 37.7$ kcal/mol ($k_{\mathrm{Me}} = 8.0\,(1) \times 10^{-6}$ s^{-1}), whereas the activation energy for MeH loss from $({}^t\mathrm{Bu_3SiNH})_3\mathrm{ZrMe}$ is $\Delta G^{\ddagger}_{96.6\,°\mathrm{C}} = 28.5$ kcal/mol (k_{Me} 1.06 (2) × 10^{-4} s^{-1}).[3] What is the origin of the >9 kcal/mol higher barrier for 1,2-elimination from Ta vs Zr? The trend in 1,2-elimination rates is also puzzling, since one might anticipate the thermolysis rates to be inversely dependent of the tantalum–carbon bond strengths. If we can assume that the Ta–C bond strengths scale to H–R bond dissociation enthalpies.[77-79] the trend observed is opposite that expected. As an example, note that 1,2-elimination of toluene (D(PhCH$_2$–H) = 88 kcal/mol)[75,80] from the benzyl derivative, 3-CH$_2$Ph, is ~100 times slower (k(CH$_2$Ph) = 1.71 (5) × 10^{-6} s^{-1}) than the related loss of benzene (D(C$_6$H$_5$–H) = 112 kcal/mol)[75,80] from 3-Ph (k_{Ph} = 1.67 (4) × 10^{-4} s^{-1}).

In order to interpret the differences in activation energy for the tantalum alkyl complexes (3-R), some assessment of ground state energies must be made. As Scheme II illustrates, $({}^t\mathrm{Bu_3SiNH})_2\mathrm{PhTa{=}NSi^tBu_3}$ (3-Ph) was exposed to excess CH$_4$ in C_6D_{12} at 182.8 °C ([CH$_4$] ~ 0.27 M)[81] to generate 3-Me. Cyclohexane-d_{12} is a convenient inert solvent because $({}^t\mathrm{Bu_3SiNH})\mathrm{Ta}({=}\mathrm{NSi^tBu_3})_2$ (4) cannot competitively activate secondary C–H bonds. Furthermore, it was assumed that this subtle change in medium and standard state would permit ready comparison with the 1,2-RH-elimination rates obtained in benzene, a presumption that was verified upon analysis of the approach to equilibrium.[76]

Formation of $({}^t\mathrm{Bu_3SiNH})_2\mathrm{MeTa{=}NSi^tBu_3}$ (3-Me) was noted, but the approach to equilibrium proved complicated due to the carbon-hydrogen bond activation of the para position of 3-Ph by $({}^t\mathrm{Bu_3SiNH})\mathrm{Ta}({=}\mathrm{NSi^tBu_3})_2$ (4), and generation of a para ditantalum phenyl derivative, $[({}^t\mathrm{Bu_3SiNH})_2\mathrm{Ta{=}NSi^tBu_3}]_2(\mu_2{:}\eta^1,\eta^1\text{-}1,4\text{-}C_6H_4)$ ((3$_2$C$_6$H$_4$). A similar species, $[({}^t\mathrm{Bu_3SiNH})_3\mathrm{Zr}]_2(\mu_2{:}\eta^1,\eta^1\text{-}1,4\text{-}C_6H_4)$, has been observed in the related zirconium system.[3,82] A diagnostic singlet was observed in the aromatic region of the ^{1}H NMR spectrum pertaining to the dimer (3)$_2$C$_6$H$_4$, but its amide and imide resonances overlapped with those of 3-Me and 3-Ph. The reaction was monitored until equilibrium was reached, as Figure 3 depicts. Simulation of the approach to equilibrium yielded rate constants consistent with the previously measured 1,2-elimination rates (Table IV). Direct calculation of the equilibrium constants ensued, and as Figure 4 indicates, the complexes (3-Me, 3-Ph, (3)$_2$C$_6$H$_4$) possess relatively similar ground state free energies. Therefore, since the ground state energy of 3-Me is only ~0.6 kcal/mol above 3-Ph, the relative 1,2-elimination rates above primarily reflect transition state energy differences.[75]

In order to corroborate the findings of the approach to equilibrium in Figure 4, a rough equilibration of $({}^t\mathrm{Bu_3SiNH})_2(\mathrm{PhCH_2})\mathrm{Ta{=}NSi^tBu_3}$ (3-CH$_2$Ph) with aryl complexes $({}^t\mathrm{Bu_3SiNH})_2(\mathrm{C_6H_4Me})\mathrm{Ta{=}NSi^tBu_3}$ (3-C$_6$H$_4$Me) was conducted by thermolysis of the former in toluene at 182.8 °C (Figure 5). The arene-activated products were treated collectively, and assumed to possess a $\Delta G^{\ddagger}$ for toluene elimination approximately equal to that for benzene elimination. While none of the 3-C$_6$H$_4$Me compounds were prepared independently, the ^{1}H NMR spectrum reveals two aryl isomers. From steric arguments and the tentative assignment of an A$_2$B$_2$ pattern, the p-tolyl species was discerned as the major isomer, but another isomer, probably the meta derivative, was also present. Since the free energy diagram shown in Figure 5 substantiated the previous study, no attempt was made to obtain more precise information. Once again, a relatively small ground state difference favoring the aryl products by ~0.4

---

(77) (a) Bryndza, H. E.; Fong, L. K.; Paciello, R. A.; Tam, W.; Bercaw, J. E. *J. Am. Chem. Soc.* **1987**, *109*, 1444–1456. (b) Bryndza, H. E.; Bercaw, J. E. *Polyhedron* **1988**, *7*, 1441–1452.

(78) Schock, L. E.; Marks, T. J. *J. Am. Chem. Soc.* **1988**, *110*, 7701–7715.

(79) For an alternative viewpoint, see: Drago, R. S.; Wong, N. M.; Ferris, D. C. *J. Am. Chem. Soc.* **1992**, *114*, 91–98.

(80) (a) Benson, S. W. *Thermochemical Kinetics*; Wiley & Sons: New York, 1968. (b) Kerr, J. A. *Chem. Rev.* **1966**, *66*, 465–500.

(81) Reamer, H. H.; Sage, B. H.; Lacey, W. N. *Ind. Eng. Chem., Chem. Eng. Data Ser.* **1958**, *3*, 240–245.

(82) For related μ-1,4-C$_6$H$_4$ compounds, see: (a) Hunter, A. D.; Szigety, A. B. *Organometallics* **1989**, *8*, 2670–2679. (b) Chukwu, R.; Hunter, A. D.; Santarsiero, B. D.; Bott, S. G.; Atwood, J. L.; Chassaignac, J. *Ibid.* **1992**, *11*, 589–597. Several examples of 1,2-activated benzenes are known. For examples, see: (c) Rausch, M. D.; Gastinger, R. G.; Gardner, S. A.; Brown, R. K.; Wood, J. S. *J. Am. Chem. Soc.* **1977**, *99*, 7870–7876. (d) Deeming, A. J. *Adv. Organomet. Chem.* **1986**, *26*, 1–96 and references therein.

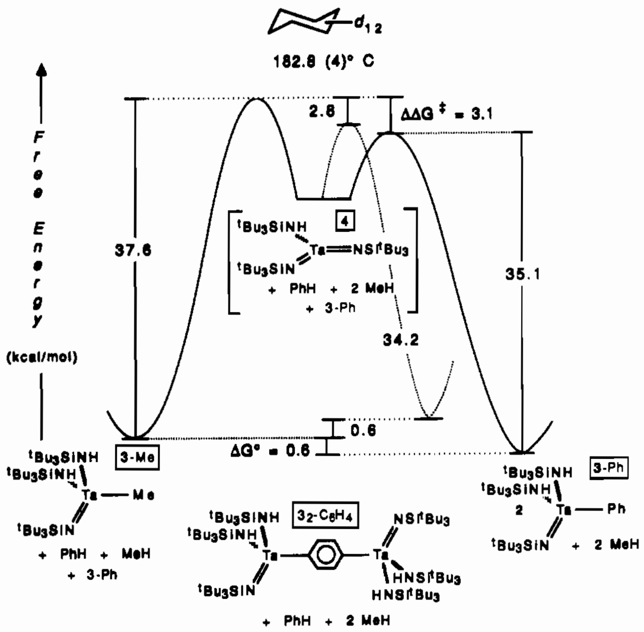

Figure 4. Free energy diagram of derived from the approach to equilibrium illustrated by Scheme II and Figure 3. The concentrations used to calculate the free energy values were obtained from the Runga–Kutta simulation of the approach to equilibrium and are referenced to a 1 M standard state. For the defined equilibrium constants, see the Experimental Section.

Scheme II

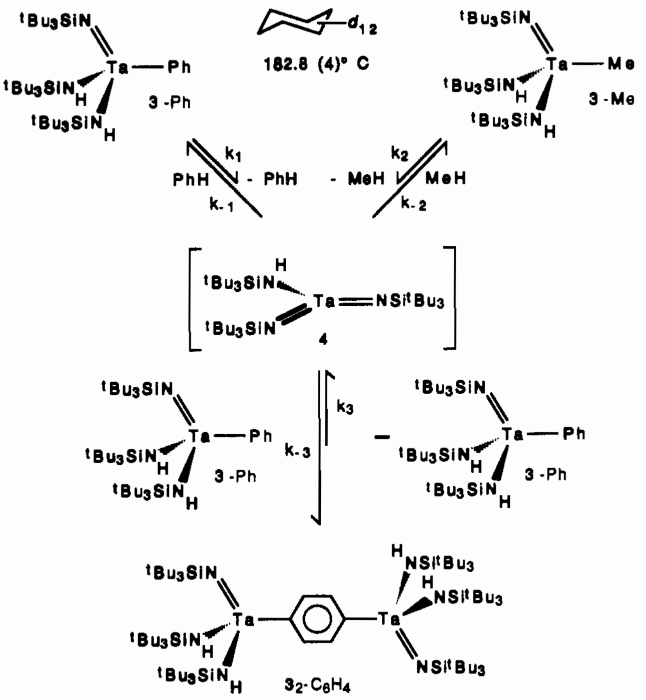

kcal/mol is overshadowed by a ~4.4 kcal/mol separation in transition state energies. It is clear that the disparity in elimination rates of benzyl vs tolyl again reflect significant differences in the respective transition states.

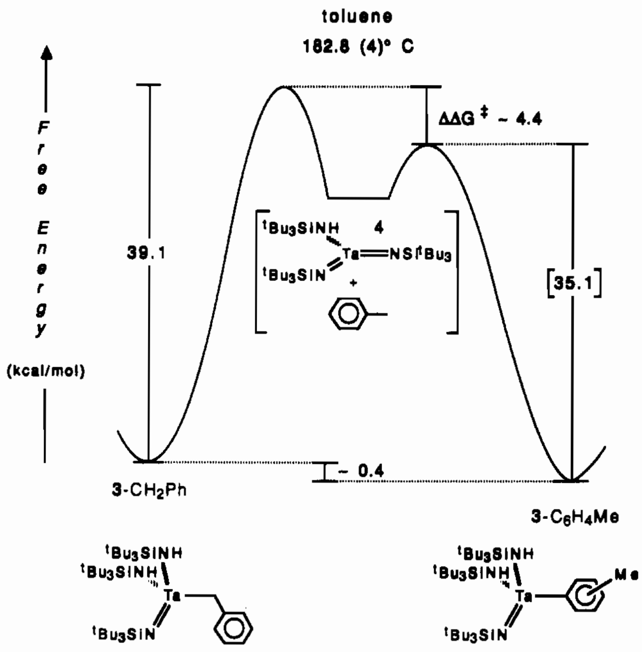

Figure 5. Free energy diagram relating $(^t\mathrm{Bu_3SiNH})_2(\mathrm{PhCH_2})\mathrm{Ta{=}NSi^tBu_3}$ (3-CH$_2$Ph) to collective aryl products $(^t\mathrm{Bu_3SiNH})_2(\mathrm{C_6H_4Me})\mathrm{Ta{=}NSi^tBu_3}$ (3-C$_6$H$_4$Me) from equilibrium and kinetic measurements. The elimination rate of 3-Ph was used to estimate that of 3-C$_6$H$_4$Me.

Discussion

The ground state and transition state energies obtained via the combination of kinetic and equilibrium data for $(^t\mathrm{Bu_3SiNH})_2\mathrm{RTa{=}NSi^tBu_3}$ (3-R) provide the rudiments necessary for an interpretation of the 1,2-RH-elimination/addition chemistry; however, several puzzles persist. A perusal of the elimination rates indicates a rough correlation with the R–H bond strength of the alkane/arene eliminated. For example, benzene, with a $D(\mathrm{C_6H_5{-}H})$ of ~112 kcal/mol is eliminated faster than neopentane ($D(\mathrm{Me_3CH_2{-}H})$ ~ 99 kcal/mol),[75,80] which in turn is eliminated faster than toluene ($D(\mathrm{PhCH_2{-}H})$ ~ 88 kcal/mol). Methane ($D(\mathrm{H_3C{-}H})$ ~ 105 kcal/mol)[75,80] is also eliminated faster than PhCH$_3$, but slower than PhH. Although neopentane elimination is somewhat swifter than MeH loss, the overall correlation is consistent with a more productlike than reactantlike transition state. An appreciable k_H/k_D of $\geq 3.4(3)$[72] at 182.8 °C corroborates the "late transition state" postulation, and implicates considerable N–H bond-breaking. Recall that a primary kinetic isotope effect should be at a maximum with an equal degree of N–H bond-breaking and C–H bond-making in a linear transition state.[75] There is a degree of common sense to the late transition state supposition, because it is reasonable to think that the putative three-coordinate complex (**4**) will be of high energy; however, the alkane/arene must also be included in an assessment of the energetics pertaining to elimination. Given the information in Figures 4 and 5, further analysis of the 1,2-elimination reaction implicates a more complicated picture.

A generalized version of the elimination/addition event is shown in eq 12, where HNM-R represents the amido–alkyl undergoing elimination (e.g., **3**-R), N=M the intermediate imide created in

$$\mathrm{HNM{-}R} \underset{\Delta H^{\ddagger}_{\mathrm{addn}}(\mathrm{R})}{\overset{\Delta H^{\ddagger}_{\mathrm{elim}}(\mathrm{R})}{\rightleftharpoons}} \mathrm{N{=}M + R{-}H} \qquad (12)$$

$$\Delta H_{\mathrm{rxn}}(\mathrm{R}) = \Delta H_f(\mathrm{prod}) - \Delta H_f(\mathrm{react}) = \Delta H_f[\mathrm{N{=}M}] + \Delta H_f[\mathrm{R{-}H}] - \Delta H_f[\mathrm{HNM{-}R}] \qquad (13)$$

$$\Delta H_{\mathrm{rxn}}(\mathrm{R}) = \Delta H^{\ddagger}_{\mathrm{elim}}(\mathrm{R}) - \Delta H^{\ddagger}_{\mathrm{addn}}(\mathrm{R}) \qquad (14)$$

the process (e.g., **4**), and RH the alkane/arene produced. The enthalpy of reaction, $\Delta H_{\mathrm{rxn}}(\mathrm{R})$ (eq 13), can be equated with the difference in enthalpies of activation for elimination and addition, $\Delta H^{\ddagger}_{\mathrm{elim}}(\mathrm{R}) - \Delta H^{\ddagger}_{\mathrm{addn}}(\mathrm{R})$ (eq 14). Since we are interested in determining the origins of the different elimination rates (i.e., $\Delta H^{\ddagger}_{\mathrm{elim}}(\mathrm{R}) - \Delta H^{\ddagger}_{\mathrm{elim}}(\mathrm{R'})$), it is unlikely that entropic factors—admittedly difficult to assess—need be seriously considered, since significant entropies are likely to cancel in the comparison. Factors such as solvation energies, which can be important, will also be considered to essentially cancel; *thus, our analysis will focus on critical bond enthalpies.*

Given that the bond dissociation enthalpy, $D(\mathrm{X{-}Y}) = \Delta H_f(\mathrm{X}) + \Delta H_f(\mathrm{Y}) - \Delta H_f(\mathrm{X{-}Y})$, the difference in enthalpies of activation for R vs. R′, $\Delta H^{\ddagger}_{\mathrm{elim}}(\mathrm{R}) - \Delta H^{\ddagger}_{\mathrm{elim}}(\mathrm{R'})$, can be defined as shown in eq 15. Given the observed $\Delta H^{\ddagger}_{\mathrm{elim}}(\mathrm{R}) - \Delta H^{\ddagger}_{\mathrm{elim}}(\mathrm{R'})$ and

$$[\Delta H^{\ddagger}_{\mathrm{elim}}(\mathrm{R}) - \Delta H^{\ddagger}_{\mathrm{elim}}(\mathrm{R'})] \sim [D(\mathrm{R'{-}H}) - D(\mathrm{R{-}H})] + [D(\mathrm{M{-}R}) - D(\mathrm{M{-}R'})] + [\Delta H^{\ddagger}_{\mathrm{addn}}(\mathrm{R}) - \Delta H^{\ddagger}_{\mathrm{addn}}(\mathrm{R'})] \quad (15)$$

$[\Delta H^{\ddagger}_{\mathrm{addn}}(\mathrm{R}) - \Delta H^{\ddagger}_{\mathrm{addn}}(\mathrm{R'})]$ values, comparisons of solution phase metal alkyl bond strengths with those of *gas-phase* carbon–hydrogen bonds can be made. Implicit in the discussion is the assumption that enthalpies and entropies of sublimation associated with the various metal–alkyl complexes (**3**-R) can be considered approximately equal.[15]

From Figure 4, $[\Delta H^{\ddagger}_{\mathrm{elim}}(\mathrm{Me}) - \Delta H^{\ddagger}_{\mathrm{elim}}(\mathrm{Ph})] = 2.5$ kcal/mol and $[\Delta H^{\ddagger}_{\mathrm{addn}}(\mathrm{Me}) - \Delta H^{\ddagger}_{\mathrm{addn}}(\mathrm{Ph})] = 3.1$ kcal/mol (~–0.36 kcal/mol are attributed to the statistics favoring benzene (6 H) vs MeH (4 H) capture). Since $[D(\mathrm{Ph{-}H}) - D(\mathrm{Me{-}H})] \sim 7$ kcal/mol, then $[D(\mathrm{HNTa{-}Me}) - D(\mathrm{HNTa{-}Ph})] \sim -7$ kcal/mol, a difference somewhat large in view of recent thermochemical studies regarding organometallic bond enthalpies, which essentially substantiate the claim that metal–carbon bond strengths are less than, but roughly correlate with, related carbon–hydrogen bond strengths.[77–79] It follows that the *difference* in metal–alkyl/aryl bond energies is expected to be smaller than the *difference* in alkane/arene CH bonds, since the $\mathrm{L}_n\mathrm{M{-}R}$ bonds are relatively smaller in magnitude. The unexpected similar magnitudes of the differences in R–H vs R′–H and Ta–R vs Ta–R′ bond strengths are directly reflected by the equilibrium shown in eq 16, with its

$$\underset{\textbf{3-Me}}{(\mathrm{^tBu_3SiNH})_2\mathrm{MeTa{=}NSi^tBu_3}} + \mathrm{PhH} \rightleftharpoons \underset{\textbf{3-Ph}}{(\mathrm{^tBu_3SiNH})_2\mathrm{PhTa{=}NSi^tBu_3}} + \mathrm{MeH} \quad (16)$$

$$\Delta H_{\mathrm{rxn}} \sim [D(\mathrm{Ta{-}Me}) - D(\mathrm{Ta{-}Ph})] + [D(\mathrm{Ph{-}H}) - D(\mathrm{Me{-}H})] \quad (17)$$

accompanying ΔH_{rxn} (eq 17) of –0.2 kcal/mol (again ~–0.36 kcal/mol of the free energy in Figure 4 are attributed to the statistics favoring benzene (6 H) vs MeH (4 H) capture), derived in the manner described above. Note that the 0.3 kcal/mol preference exhibited by **4** in activating one of the six C–H bonds of benzene vs the lone *p*-phenyl C–H bond of **3**-Ph to give $(\mathbf{3})_2\mathrm{C_6H_4}$ can be easily considered a consequence of statistics.

The energy diagram reflecting benzyl vs aryl elimination possesses similar features to the scenario espoused above. From Figure 5, $[\Delta H^{\ddagger}_{\mathrm{elim}}(\mathrm{CH_2Ph}) - \Delta H^{\ddagger}_{\mathrm{elim}}(\mathrm{Ph})] \sim 4.0$ kcal/mol (recall that the elimination rate for **3**-Ph was used) and $[\Delta H^{\ddagger}_{\mathrm{addn}}(\mathrm{PhCH_2{-}H}) - \Delta H^{\ddagger}_{\mathrm{addn}}(\mathrm{MeC_6H_4H})] \sim 4.4$ kcal/mol. Since $[D(\mathrm{Ar{-}H}) - D(\mathrm{PhCH_2{-}H})] \sim 24$ kcal/mol, then $[D(\mathrm{HNTa{-}CH_2Ph}) - D(\mathrm{HNTa{-}Ar})] \sim -24$ kcal/mol, another large difference that contradicts current dogma regarding metal–carbon bond strengths.[77–79] This value may also be directly obtained from the rough measurement (eq 19) of the equilibrium indicated by eq 18. Again, the *difference* in Ta–C bond strengths is similar to the *difference* in related carbon–hydrogen bonds. In eq 18, no hydrocarbon is included in the equilibrium, because both **3**-CH$_2$Ph and the various aryls, **3**-C$_6$H$_4$Me, eliminate the same molecule, toluene. Since comparable free energy pictures are obtained for the Me vs Ph and benzyl vs aryl activations (i.e., minor ground state differences that ultimately relate to large differences in $D(\mathrm{Ta{-}R}) - D(\mathrm{Ta{-}R'})$), the assumption that entropic factors and

$$\underset{\textbf{3-CH}_2\textbf{Ph}}{(\mathrm{^tBu_3SiNH})_2(\mathrm{PhCH_2})\mathrm{Ta{=}NSi^tBu_3}} \rightleftharpoons \underset{\textbf{3-C}_6\textbf{H}_4\textbf{Me}}{(\mathrm{^tBu_3SiNH})_2(\mathrm{MeC_6H_4})\mathrm{Ta{=}NSi^tBu_3}} \quad (18)$$

$$\Delta H_{\mathrm{rxn}} \sim [D(\mathrm{Ta{-}CH_2Ph}) - D(\mathrm{Ta{-}C_6H_4Me})] + [D(\mathrm{MeC_6H_4{-}H}) - D(\mathrm{PhCH_2{-}H})] \quad (19)$$

heats of solvation are either minimal, or essentially cancel in comparison, gains some credence.

In order for a late transition state to be operative, the difference in energy between the transition state and intermediate state (i.e., **4** + RH) must be small, whereas the energy difference between ground and transition states must be large.[75] It follows that $[\Delta H^{\ddagger}_{\mathrm{addn}}(\mathrm{R}) - \Delta H^{\ddagger}_{\mathrm{addn}}(\mathrm{R'})]$ should also be small and substantially less than $[\Delta H^{\ddagger}_{\mathrm{elim}}(\mathrm{R}) - \Delta H^{\ddagger}_{\mathrm{elim}}(\mathrm{R'})]$. If the depth of the well in which **4** + RH resides is significant neither will be relevant. The key observation in this study concerns the ability of $(\mathrm{^tBu_3SiNH})\mathrm{Ta}(=\mathrm{NSi^tBu_3})_2$ (**4**) to *discriminate* between the C–H bonds of methane vs. benzene, as evidenced by the $[\Delta H^{\ddagger}_{\mathrm{addn}}(\mathrm{Me}) - \Delta H^{\ddagger}_{\mathrm{addn}}(\mathrm{Ph})]$ value of ~3.1 kcal/mol. If the transition states for **4**···Me-H or **4**···Ph-H were truly near those of intermediates **4** plus Me–H or Ph–H, it is unlikely that the magnitude of $\Delta\Delta H^{\ddagger}_{\mathrm{addn}}$ (MeH vs PhH) would be that large. Note that a similar transition state differentiation is obtained with toluene as the substrate; **4** selectively adds aryl over benzylic C–H bonds ($\Delta\Delta H^{\ddagger}_{\mathrm{addn}}$ (ArCH$_2$–H vs Ar–H) ~ 4.4 kcal/mol). Nor is the differentiation limited to cases involving arene vs. alkane (or benzyl) activation. Recall that the approach to equilibrium in Figure 4 was conducted in neat cyclohexane-d_{12}, yet MeH and benzene clearly compete successfully for **4** with respect to activation of the solvent. A rough calculation indicates that **4** discriminates for MeH over CyH by >6.5 kcal/mol.[83] Furthermore, since no deuteration of the amide bonds of **3**-Me and **3**-Ph was observed in the course of this experiment, no appreciative addition of $\mathrm{C_6D_{12}}$ to **4** was found; hence, the above estimate is undoubtedly a conservative one.

Since the late transition state postulation, while consistent with the rough inverse correlation of 1,2-RH-elimination rate vs Ta–C bond energy, is less than satisfactory, two key explanations appear plausible (Figure 6): (1) the intermediate **4** + alkane/arene state is lower in energy than initially proposed (A); (2) the alkane/arene first achieves a *binding* configuration, another intermediate state (**4**-RH), prior to C–H bond activation (B). This rationale is attractive in view of the hypotheses regarding alkane complexes in group 9 C–H activating systems,[14] recently observed gas-phase alkane complexes,[36] and the plethora of stable and transient η^2-arene complexes.[15,84] In this system, such binding would be significantly different because the metal center of **4** is d^0, but since the 3-coordinate species is expected to be very electrophilic, with the localized $\mathrm{d}_{z^2}/\mathrm{p}_z$ hybrid serving as the critical orbital, an interaction akin to that of an ion–dipole complex is compelling.[40] In either case, the strength of the C–H bond formed in the elimination step may still play a important role in establishing the energy of the intermediate state, whether or not R–H is bound to **4**. Note that in one limit of scenario B, the generation of free $(\mathrm{^tBu_3SiNH})\mathrm{Ta}(=\mathrm{NSi^tBu_3})_2$ (**4**) need not be postulated; an

---

(83) Using the density of $\mathrm{C_6H_{12}}$, correcting for deuterium, and assuming it is relatively insensitive to temperature, the density of $\mathrm{C_6D_{12}}$ is roughly 0.89 g/mL and neat cyclohexane-d_{12} is ~9.3 M. Taking the selectivity of **4** for MeH over CyH to be at least 100 (presumably a measurable quantity by ^{1}H NMR), then $k(\mathrm{CH_4})/k(\mathrm{C_6D_{12}}) \sim (k_{\mathrm{MeH}}[\mathbf{4}][\mathrm{MeH}]/(k_{\mathrm{CyH}}[\mathbf{4}][\mathrm{CyH}]) \sim (k_{\mathrm{MeH}}[\mathbf{4}][0.7])/(k_{\mathrm{CyH}}[\mathbf{4}][9.3]) > 100$ and $k_{\mathrm{MeH}}/k_{\mathrm{CyH}} > 1300$. Since $k_{\mathrm{MeH}}/k_{\mathrm{CyH}} = \exp[(\Delta G^{\ddagger}_{\mathrm{CyH}} - \Delta G^{\ddagger}_{\mathrm{MeH}})/RT] > 1300$, then $\Delta G^{\ddagger}_{\mathrm{CyH}} - \Delta G^{\ddagger}_{\mathrm{MeH}} > 6.5$ kcal/mol at 456 K.

(84) For recent arene intermediates preceding C–H activation, see: (a) Belt, S. T.; Dong, L.; Duckett, S. B.; Jones, W. D.; Partridge, M. C.; Perutz, R. N. *J. Chem. Soc., Chem. Commun.* **1991**, 266–269. (b) Jones, W. D.; Dong, L. *J. Am. Chem. Soc.* **1989**, *111*, 8722–8723.

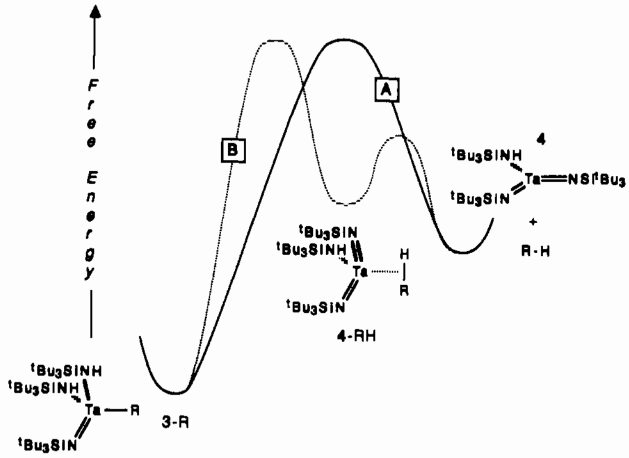

Figure 6. Plausible pathways for alkane elimination: Path A manifests a lower than originally anticipated energy state for **4** + RH; path B indicates a d^0 alkane/arene binding intermediate.

associative displacement of RH from **4**-RH by R'H to yield **4**-R'H is a viable alternative, one fully consistent with the kinetic and thermodynamic data, yet somewhat unlikely from the standpoint of sterics.

In both free energy diagrams, the ground-state energies of the alkyl (**3**-Me + PhH) or benzyl (**3**-CH_2Ph) derivatives were surprisingly similar to related aryl (**3**-Ph + MeH; **3**-C_6H_4Me) species principally because the differences in metal–carbon energies proved to be larger than anticipated. Schock and Marks[78] have observed that the Hf–CH_3 bond strength rises from ~69 kcal/mol by ~1–2 kcal/mol with increasing alkoxide substitution in $Cp^*HfMe_x(OC_6F_5)_{3-x}$ (x = 1–3), suggesting that electronegative substituents on a metal enhance metal–alkyl bond strength through an increasing ionic contribution. However, it is likely that tantalum–carbon bonds are inherently somewhat weaker than corresponding hafnium–carbon bonds, and it is highly unlikely that even a dramatic change in coordination sphere (e.g., $({}^tBu_3SiNH)_2RTa{=}NSi^tBu_3$ (**3**-R) vs $Cp^*HfMe(OC_6F_5)_2$) would enable tantalum–carbon bonds to approach the strength of related carbon–hydrogen bonds.[75,80]

In order to explain the above discrepancy, two factors may play important roles. The premise that metal–carbon bond strengths parallel those of the respective carbon–hydrogen bonds rests with the contention that the enthalpies of the alkyl fragments in common are virtually equivalent. If π-donation from a phenyl or aryl unit to the electrophilic metal center containing an imido functionality is appreciable, then an additional stabilization may be present due to resonance I, as illustrated in Figure 7. In studies of $Cp^*(Me_3P)MRH$ (M = Rh, Ir) systems that mediate C–H bond activation chemistry, Jones and Feher estimated the Rh–Ph bond enthalpy to be 12.6 kcal/mol greater than the Rh–Me,[15] and Bergman et al. have shown that the Ir–Ph bond (80.6 kcal/mol) is substantially stronger than the Ir–Cy linkage (50.8 kcal/mol).[85] The corresponding benzene C–H bond is only ~7 kcal/mol greater than a Me–H bond and ~17 kcal/mol stronger than a cyclohexane C–H bond; thus, it appears that a metal–phenyl bond may be especially strong. For the late metal M–Ph groups, a resonance stabilization from a $M(d\pi)\rightarrow Ph(\pi^*)$ interaction could contribute to inordinately strong metal–phenyl bonds. However, in studying the aryl rotation rates in $Cp^*(R_3P)Rh(aryl)X$,[86] Jones and Feher uncovered little evidence of rhodium–aryl π-interactions; hence, it is conceivable that the previously mentioned assumptions (i.e., heats and entropies of solvation, sublimation, etc.) lack the required validity in these systems. Alternatively, an electronic component to an aryl rotation barrier may not be discernible provided the π-type orbitals of the $Cp^*(R_3P)RhX$ fragment are cylindrically symmetric with respect to the aryl.

C_α–H bond strengths may be *lowered* due to stabilization akin to that of an allylic radical, as shown in II. Additional resonance stabilization where X = Ph (II) may be operative in enhancing the discrepancy between predicted and estimated bond strength differences. Other perturbations by the electropositive tantalum center on the enthalpies of the alkyl/aryl fragments, such as hyperconjugative effects, may also contribute, but I and II appear most transparent. Steric factors must play significant roles in the bond enthalpies of the Ta–R bonds and fragment enthalpies, but in the absence of steric corrections applicable to this particular system, a discussion of these contributions is unwarranted. For example, Ph should surely be a larger substituent than Me, yet it is the unexpectedly *low* energy of **3**-Ph + MeH (relative to **3**-Me + PhH) that requires rationalization.

There is a counterargument to the thesis that a metal–phenyl bond is inordinately strong. Consider the graph in Figure 8, which illustrates a correlation between D(C–H) and the observed differences in Ta–Ph vs Ta–R (R = Me, CH_2Ph) bond enthalpies taken from eqs 17 and 19. A crude minimum difference between Ta–Ph and the unobserved Ta–Cy may be derived[87] and is indicated by an open circle; a rough minimum difference pertaining to Ta–$CH_2{}^tBu$ can be similarly estimated.[88] While the data is admittedly sparse, the graph shows that the Ta–Ph bond enthalpy need not be extraordinary. From examination of the data, a plausible relationship between metal–carbon and carbon–hydrogen bond enthalpies of the form $D(\text{Ta–C}) \sim \alpha[D(\text{C–H})] + \beta + A(\text{steric factor})$ can be imagined. An "A-value" for specific alkyls would presumably be largest for secondary (e.g., Cy) and neopentyl fragments, and β would be a constant for all R. While augmented by a steric factor, this equation essentially parallels those based on Pauling electronegativities that have recently been promoted by Schock and Marks to detail early transition metal and actinide bond strengths.[78] Simply stated, the differences in D(Ta–R) manifest the differences in heats of formation of the various alkyl radicals, R$^\bullet$ ($\alpha \sim 1$). It is clear that more alkyl vs alkyl comparisons must be undertaken in order to prove whether Figure 8 is simply manifesting the special cases highlighted by Figure 7.

One remaining puzzle concerns the apparent >9 kcal/mol higher barrier for 1,2-RH-elimination from $({}^tBu_3SiNH)_2RTa{=}NSi^tBu_3$ (**3**-R) vs. $({}^tBu_3SiNH)_3ZrR$ to generate $({}^tBu_3SiNH)Ta({=}NSi^tBu_3)_2$ (**4**) vs $({}^tBu_3SiNH)_2Zr{=}NSi^tBu_3$. A review of the binding in the equatorial plane of $(py)_2MeTa({=}NSi^tBu_3)_2$ (**2**$(py)_2$) provides some rationale. Due to symmetry constraints, contributions from π-bonding of the two imido ligands in **2**$(py)_2$ is limited to 6 e$^-$ donation, instead of the maximum of 8. The situation is mirrored in purported intermediate **4**, assuming pseudo-trigonal symmetry, with the additional problem of accommodating a third π-donor in the form of the remaining amide. In contrast, one less π-interaction is attributed to the putative zirconium transient, $({}^tBu_3SiNH)_2Zr{=}NSi^tBu_3$. It is

---

(85) Nolan, S. P.; Hoff, C. D.; Stoutland, P. O.; Newman, L. J.; Buchanan, J. M.; Bergman, R. G.; Yang, G. K.; Peters, K. S. *J. Am. Chem. Soc.* **1987**, *109*, 3143–3145.

(86) Jones, W. D.; Feher, F. J. *Inorg. Chem.* **1984**, *23*, 2376–2388.

(87) Thermolysis of **3**-Ph (0.030 M) in C_6D_{12} (~9.3 M) at 182.8 °C results in no **3**-Cy. Assuming that 1% of **3**-Cy could have been detected, K_{eq} for **3**-Ph + CyH $\rightleftharpoons$ **3**-Cy + PhH = [**3**-Cy][PhH]/[**3**-Ph][CyH] = [0.0003][0.0003]/[0.0297][9.3] = 3.26×10^{-7}; $\Delta G^\circ = -RT \ln K_{eq} = -(0.001\,987\ \text{kcal/(K·mol)})(456\ \text{K}) \ln [3.26 \times 10^{-7}]$ = 13.5 kcal/mol, a minimum value. Since D(Cy–H) = 95 and D(Ph–H) = 112 kcal/mol, an equation analogous to eqs 17 and 19 gives [D(Ta-Ph) – D(Ta-Cy)] = 30.5 kcal/mol.

(88) Thermolysis of **3**-$CH_2{}^tBu$ (0.028 M) in C_6D_6 (~11.2 M) at 182.8 °C results in **3**-$(ND)_2Ph$-d_5. Assuming that 1% of **3**-$CH_2{}^tBu$ could have been detected, K_{eq} for **3**-$CH_2{}^tBu$ + PhH $\rightleftharpoons$ **3**-Ph + Me_4C = [3-Ph][Me_4C]/[3-$CH_2{}^tBu$][PhH] = ([0.02772][0.02772])/([0.00028][11.2]) = 0.245; $\Delta G^\circ = -RT \ln K_{eq} = -(0.001\,987$ kcal/(K·mol) (456 K) ln [0.245] = 1.3 kcal/mol, a minimum value. Since $D({}^tBuCH_2\text{–H})$ = 99 and D(Ph–H) = 112 kcal/mol, an equation analogous to eqs 17 and 19 gives [D(Ta–Ph) – D(Ta–$CH_2{}^tBu$)] = 11.7 kcal/mol.

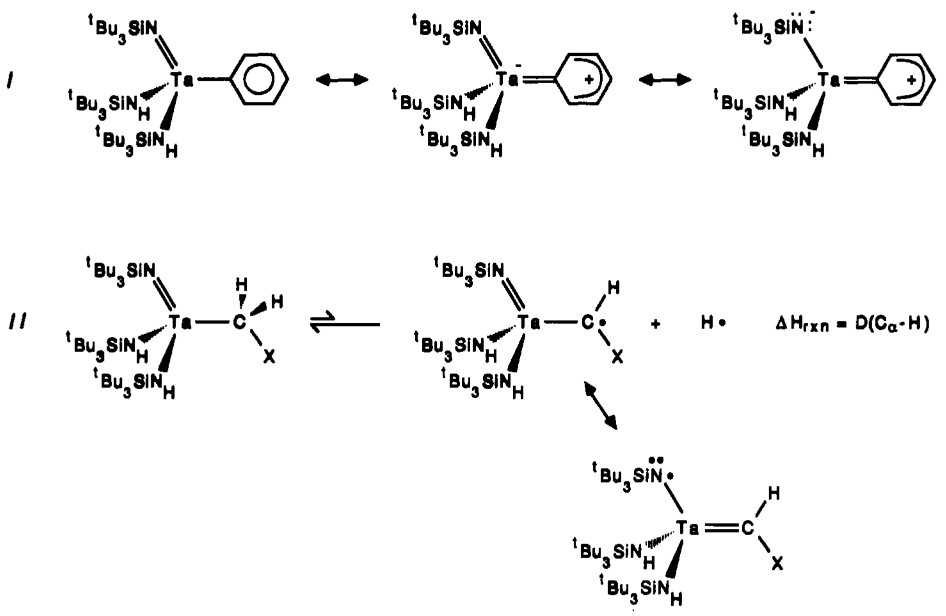

Figure 7. Possible resonance contributions may increase the Ta–Ph bond strength according to I. Allylic stabilization may lower C_α-H bond strengths according to II.

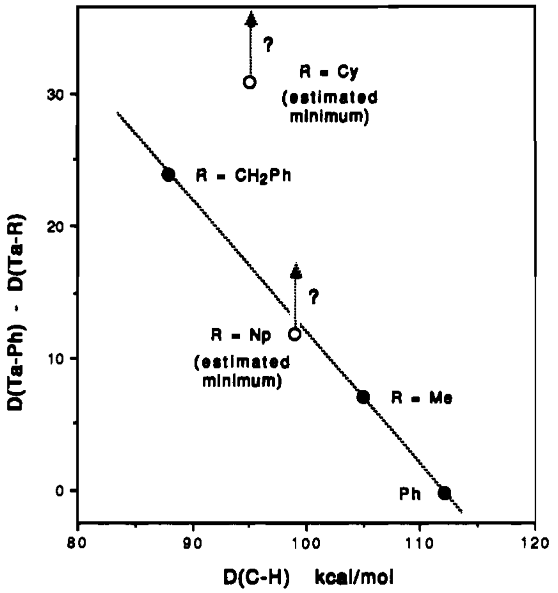

Figure 8. Correlation between D(C–H) of the eliminated alkane/arene and D(Ta–Ph) – D(Ta–R). See text for details.

possible that the inability of the tantalum center to comply with the π-bonding requirements of the tantalum intermediate (**4**) renders it inherently of higher energy than its zirconium congener. Furthermore, the orbitals of zirconium are more radially extent than those of tantalum; hence, the electrophilicity of the former may be more readily transmitted to substrate alkanes and arenes.

A second factor relevant to the difference between Ta and Zr elimination rates concerns the polarity of the transition state for elimination.[3] It is probable that the zirconium–carbon bonds possess a higher ionic contribution than corresponding tantalum bonds. If the energy of the transition state depends on the polarity of these bonds, then it is logical to expect the Zr eliminations to be more expedient. For example, if elimination bears a relationship to protonation of the metal–carbon bond, in this case by an "acidic" amido proton, swifter elimination may be expected for a more "basic" alkyl or aryl bond. It is instructive to view this point via the microscopic reverse, the addition of alkane or arene to an electrophilic three-coordinate imido intermediate. The zirconium center in $(^t\text{Bu}_3\text{SiNH})_2\text{Zr}{=}\text{NSi}^t\text{Bu}_3$ should be a more effective electrophile than **4** in serving to polarize the carbon–hydrogen bond prior to addition.

The only experiment designed to vary the electrophilicity at tantalum, the thermolysis of $(^t\text{Bu}_3\text{SiNH})(^t\text{Bu}_3\text{SiO})\text{MeTa}{=}\text{NSi}^t\text{Bu}_3$ (**5-Me**), is unfortunately moot. Loss of MeH from **5-Me** is about 8-fold slower than loss of methane from **3-Me**. Although putative intermediate $(^t\text{Bu}_3\text{SiO})\text{Ta}({=}\text{NSi}^t\text{Bu}_3)_2$ (**6**) is predicted to be more electrophilic than its amide counterpart (**4**) on electronegativity grounds, it possesses more pπ–dπ interactions because of the additional oxygen lone pair. In addition, the ground state of **5-Me** may be electronically and sterically stabilized relative to **3-Me**, hence any conclusions drawn from this experiment are tenuous at best.

Summary

While our comprehension of 1,2-RH-elimination from $(^t\text{Bu}_3\text{SiNH})_2\text{RTa}{=}\text{NSi}^t\text{Bu}_3$ (**3-R**) and 1,2-RH-addition to $(^t\text{Bu}_3\text{SiNH})\text{Ta}({=}\text{NSi}^t\text{Bu}_3)_2$ (**4**) remains incomplete, a better understanding of the fundamental steps of the process has been achieved. Although formally it is improper to attribute the 1,2-elimination/addition to a late transition state, influences that skew ground-state energies from those expected are also contributing to the discrimination observed by **4** in attacking carbon–hydrogen bonds. The C–H bond strength of the alkane/arene generated upon elimination contributes importantly in determining the energy of the intermediate (**4** + RH) state—a state that is of lower energy than originally anticipated—and therefore the transition state critical to C–H bond activation. This study has reaffirmed the importance of producing an electrophilic site in order to capture the electon density in a carbon–hydrogen bond. Furthermore, this site must be localized in order to maximize the radial extention needed to strongly interact with substrates that are difficult to polarize.

Greater insight into the relative ground-state and transition-state energies are needed to fully comprehend the origins of these intriguing reactions. Unfortunately, the limitations of the tantalum system, principally the high temperatures required to provide the reactive intermediate **4**, have constrained our interpretations. We hope that kinetic and thermodynamic studies of the $(^t\text{Bu}_3\text{SiNH})_3\text{ZrR}$ 1,2-RH-eliminations will provide the insight necessary to provide a more concrete overview of this reaction. Substantial synthetic diversity provides a greater scope of 1,2-RH-eliminations and pertinent structural studies, while kinetic isotope measurements on both the elimination from $(^t\text{Bu}_3\text{SiNH})_3\text{ZrR}$ and the addition of RH to $(^t\text{Bu}_3\text{SiNH})_2\text{Zr}{=}\text{NSi}^t\text{Bu}_3$ promise to shed significant light on this reaction. These investigations[3] and those of a related (^{t}Bu$_3$SiO)$_2$RTi(NHSi^{t}Bu$_3$) system will be completed in due course.

Experimental Section

General Considerations. All manipulations were performed using either glovebox or high-vacuum-line techniques. Hydrocarbon solvents containing 1–2 mL of added tetraglyme were distilled under nitrogen from purple benzophenone ketyl and vacuum transferred from same prior to use. Benzene-d_6, cyclohexane-d_{12}, and pyridine were dried over activated 4-Å molecular sieves, vacuum transferred, and stored under N$_2$; THF and THF-d_8 were dried over sodium benzophenone ketyl. All glassware was base-washed and oven-dried, and NMR tubes were additionally flamed under dynamic vacuum. Methane (Matheson) was used as received. TaCl$_5$ (Pressure Chemical Co.) was used as received. LiNHSi^{t}Bu$_3$[63,64] and Me$_3$TaCl$_2$[62] were prepared according to published procedures.

^{1}H and ^{13}C{^{1}H} NMR spectra were obtained using Varian XL-200 and XL-400 spectrometers. Infrared spectra were recorded on a Mattson FT-IR interfaced to an AT&T PC7300 computer or a Perkin Elmer 299B spectrophotometer. The Runge Kutta kinetics simulation program used was written by Prof. Barry K. Carpenter of Cornell University. Analyses were performed by Texas Analytical Labs, Stafford, TX, or Oneida Research Services, Whitesboro, NY.

Synthetic Procedures. 1. (^{t}Bu$_3$SiNH)Me$_2$Ta=NSi^{t}Bu$_3$ (1). To a flask containing a solution of ^{t}Bu$_3$SiNHLi (1.677 g, 7.530 mmol) in hexanes (30 mL) at −15 °C was added TaMe$_3$Cl$_2$ (1.125 g, 3.787 mmol, 0.5 equiv). The resulting brown slurry was warmed to 25 °C and stirred for an additional 1.5 h. The reaction mixture was filtered and extracted with hexanes (5 × 10 mL). The resulting brown filtrate was concentrated to 6 mL, cooled to −78 °C for 0.5 h, and filtered to yield colorless, crystalline **1** (1.529 g, 63%). IR (Nujol, cm^{-1}): 3286 (m, NH), 1365 (m), 1193 (m, sh), 1184 (m), 1165 (m), 1149 (s, br), 1065 (m, br), 1012 (m), 932 (m), 862 (s, br), 818 (s), 722 (m), 620 (s, br). Anal. Calcd for TaC$_{26}$H$_{61}$N$_2$Si$_2$: C, 48.88; H, 9.62; N, 4.38. Found: C, 47.36; H, 9.23; N, 4.30.

2. (^{t}Bu$_3$SiNH)Me$_2$(py)Ta=NSi^{t}Bu$_3$ (1-py). To a flask containing (^{t}Bu$_3$SiNH)Me$_2$Ta(=NSi^{t}Bu$_3$) (310 mg, 0.485 mmol) at −78 °C was added 10 mL of pyridine by vacuum distillation. The solution was thawed and stirred for 0.5 h, then the solvent was removed by vacuum transfer, and the resulting off-white product was slurried in hexanes. After filtration and five 10-mL washes with hexanes, the extracts were combined, concentrated to 2 mL, cooled to −78 °C for 0.5 h, and filtered. An off-white powder was obtained (187 mg, 0.268 mmol, 55%). IR (Nujol, cm^{-1}): 3285 (m, NH), 1610 (s), 1542 (w), 1450 (s), 1420 (m), 1365 (m), 1235 (w), 1220 (m), 1185 (w), 1166 (m), 1135 (s, br), 1066 (s, br), 1012 (s), 932 (m), 856 (s, br), 817 (s), 756 (m), 696 (m), 618 (s). Anal. Calcd for TaC$_{31}$H$_{66}$N$_3$Si$_2$: C, 53.34; H, 9.53; N, 5.60. Found: C, 50.83; H, 9.12; N, 5.56.

3. (py)$_2$MeTa(=NSi^{t}Bu$_3$)$_2$ (2(py)$_2$). To a glass bomb containing (^{t}Bu$_3$SiNH)Me$_2$Ta=NSi^{t}Bu$_3$ (**1**, 1.516 g, 2.373 mmol) at −78 °C was added 40 mL of pyridine via vacuum transfer. The reactor was immersed in an oil bath at 95 °C for 20 h and the colorless solution became deep yellow. The volatiles were removed, passed through a series of dry ice/acetone traps and admitted to a Toepler pump; 1.0 equiv of methane (IR) was produced. The resulting brown residue was dissolved in benzene and filtered. Concentration of 2 mL resulted in the formation of yellow crystals, which were isolated by filtration (989 mg). A second crop produced an additional 272 mg (1.261 g, 68% total). ^{1}H NMR spectroscopy showed 5% unidentified impurities present even after subsequent recrystallization. IR (Nujol, cm^{-1}): 3015 (w), 3080 (w), 2700 (w), 1980 (w), 1925 (w), 1850 (w), 1643 (w), 1602 (s), 1567 (w), 1538 (w), 1480 (s), 1441 (s), 1353 (m), 1230 (w), 1214 (m), 1180 (m), 1150 (m), 1130 (s), 1085 (m), 1040 (s, br), 1005 (s), 930 (m), 875 (w), 812 (s), 730 (m), 725 (m), 695 (s), 670 (w), 627 (m). Anal. Calcd for TaC$_{35}$H$_{67}$N$_4$Si$_2$: C, 53.82; H, 8.65; N, 7.17. Found: C, 53.65; H, 8.75; N, 7.08.

4. (THF)$_2$MeTa(=NSi^{t}Bu$_3$)$_2$ (2(THF)$_2$). Thermolysis of a THF-d_8 solution containing (^{t}Bu$_3$SiNH)Me$_2$Ta=NSi^{t}Bu$_3$ (**1**) in a sealed, 5-mm flame-dried NMR tube at 100 °C for several days gave a yellow solution. Monitoring by ^{1}H NMR spectroscopy showed the disappearance of starting material and the growth of one major product, prompting a larger scale effort. To a glass bomb containing **1** (300 mg, 0.469 mmol) at −78 °C was added 15 mL of THF via vacuum transfer. The reactor was immersed in an oil bath at 105 °C for 68 h, and the colorless solution turned light brown. The volatiles were removed, passed through a series of dry ice/acetone traps and admitted to a Toepler pump; 0.56 equiv of methane (IR) was produced. The resulting oily solid was dissolved in benzene, filtered, and triturated three times in 10 mL of benzene and then once in hexanes (10 mL). The hexanes solution was concentrated to 3 mL, cooled to −78 °C, and filtered to obtain off-white microcrystals of **3** (46 mg, 0.060 mmol, 13%). IR (Nujol, cm^{-1}): 1470 (s, br), 1460 (s, sh), 1390 (m, sh), 1380 (s), 1360 (m), 1295 (w), 1245 (w), 1170 (w), 1155 (m, sh), 1142 (s), 1045 (s, br), 1009 (s, br), 932 (m), 920 (m), 867 (s), 850 (m, sh), 818 (s), 722 (w), 674 (w), 610 (s). Anal. Calcd for TaC$_{33}$H$_{73}$N$_2$O$_2$Si$_2$: C, 51.67; H, 9.59; N, 3.65. Found: C, 51.49; H, 9.66; N, 3.56.

5. (^{t}Bu$_3$SiNH)$_2$ClTa=NSi^{t}Bu$_3$ (3-Cl). To a flask containing a slurry of LiNHSi^{t}Bu$_3$ (2.109 g, 9.513 mmol, 4.0 equiv) in 50 mL of diethyl ether at −78 °C was added TaCl$_5$ (853 mg, 2.381 mmol). The slurry warmed slowly to 25 °C while stirring and turned from pale yellow to olive green and then back to pale yellow. The solution was stirred at room temperature under argon for an additional 12 h before removing the solvent under vacuum. The solid was extracted and filtered five times with 20-mL portions of hexanes followed by concentration to 10 mL. Upon the filtrate was cooled to −78 °C, colorless crystals were obtained by filtration (1.685 g, 82%). Stirring for shorter times resulted in yields of 50–60%. IR (Nujol, cm^{-1}): 3285 (w, NH), 3250 (w, NH), 3235 (w, NH), 1155 (m), 1100 (s, br), 1080 (m), 1014 (m), 968 (w), 935 (m), 857 (s), 816 (s, br), 720 (m), 622 (s, br). Anal. Calcd for TaC$_{36}$H$_{83}$N$_3$ClSi$_3$: C, 50.35; H, 9.74; N, 4.89. Found: C, 50.45; H, 9.74; N, 4.31.

6. (^{t}Bu$_3$SiNH)$_2$MeTa=NSi^{t}Bu$_3$ (3-Me). To a flask containing (^{t}Bu$_3$SiNH)$_2$ClTa=NSi^{t}Bu$_3$ (**3-Cl**; 998 mg, 1.162 mmol) was added 25 mL of hexanes via vacuum distillation. AlMe$_3$ (1.05 equiv, 0.61 mL of 2.0 M solution in hexanes) was syringed in under argon counterflow at −78 °C. The solution was warmed to 25 °C and stirred for ~12 h before the volatiles were removed under vacuum. The resulting white solid was extracted and washed with five 10-mL portions of hexanes, and the combined extracts were concentrated to 5 mL and cooled to −78 °C. Colorless crystals were collected by filtration (756 mg, 0.902 mmol, 78%). IR (Nujol, cm^{-1}): 3260 (w, NH), 3245 (m, NH), 1159 (m), 1184 (m), 1099 (s, br), 1021 (s), 1001 (s, br), 952 (m), 852 (s), 814 (s, br), 587 (m). Anal. Calcd for TaC$_{37}$H$_{86}$N$_3$Si$_3$: C, 53.01; H, 10.34; N, 5.01. Found: C, 52.68; H, 10.29; N, 4.86.

7. (^{t}Bu$_3$SiNH)$_2$PhTa=NSi^{t}Bu$_3$ (3-Ph). To a flask containing (^{t}Bu$_3$SiNH)$_2$ClTa=NSi^{t}Bu$_3$ (**3-Cl**; 1.000 g, 1.164 mmol) at −78 °C was added 15 mL of hexanes by vacuum distillation. PhLi (1.1 equiv, 0.71 mL of 1.8 M solution in Et$_2$O/cyclohexane) was syringed in under argon counterflow at −78 °C. The resulting reddish solution was warmed to 25 °C and stirred for ~12 h. The solution was filtered, washed once with 10 mL of hexanes, concentrated to 5 mL, and cooled, to −78 °C for 1 h. Filtration yielded 474 mg of colorless crystals; a second crop provided an additional 191 mg (665 mg, 64% total). IR (Nujol, cm^{-1}): 3270 (m, NH), 3255 (w, NH), 3220 (m, NH), 3185 (w, NH), 1415 (w), 1362 (m), 1188 (w), 1149 (w), 1135 (m), 1085 (s, br), 1061 (m), 1008 (m), 989 (m), 928 (m), 850 (s, br), 815 (s, br), 719 (m), 692 (m), 648 (m), 614 (s, br). Anal. Calcd for TaC$_{42}$H$_{88}$N$_3$Si$_3$: C, 56.03; H, 9.85; N, 4.67. Found: C, 55.65; H, 10.61; N, 4.47.

8. (^{t}Bu$_3$SiNH)$_2$(PhCH$_2$)Ta=NSi^{t}Bu$_3$ (3-CH$_2$Ph). To a flask containing (^{t}Bu$_3$SiNH)$_2$ClTa=NSi^{t}Bu$_3$ (**3-Cl**; 500 mg, 0.582 mmol) in 15 mL of toluene at 25 °C was added solid PhCH$_2$K (76 mg, 0.58 mmol), which slowly dissolved to give an orange-red solution. The solution was stirred for ~12 h before removal of the solvent in vacuum. The resulting orange solid was extracted and washed three times in 10 mL of hexanes, and the combined extracts were concentrated to 3 mL. When this was cooled to −78 °C, white microcrystals were collected by filtration (282 mg, 0.298 mmol, 51%). IR (Nujol, cm^{-1}): 3260 (w, NH), 3222 (m, NH), 1602 (m), 1595 (m, sh), 1367 (m), 1205 (m), 1146 (m), 1099 (s, br), 1030 (w), 1012 (m), 992 (w), 935 (m), 855 (s, br), 820 (s, br), 747 (m), 698 (m), 620 (s, br). Anal. Calcd for TaC$_{43}$H$_{90}$N$_3$Si$_3$: C, 56.48; H, 9.92; N, 4.59. Found: C, 56.32; H, 10.07; N, 4.41.

9. (^{t}Bu$_3$SiNH)$_2$(^{t}BuCH$_2$)Ta=NSi^{t}Bu$_3$ (3-CH$_2$^{t}Bu). To a flask containing an intimate mixture of (^{t}Bu$_3$SiNH)$_2$ClTa=NSi^{t}Bu$_3$ (**3-Cl**; 721 mg, 0.839 mmol) and ^{t}BuCH$_2$Li (66 mg, 0.85 mmol) at −78 °C was added 25 mL of Et$_2$O by vacuum distillation. The solution was warmed to 25 °C and stirred for a total of 4.5 h and the solvent removed. A ^{1}H NMR spectrum of the crude mixture revealed that all of the ^{t}BuCH$_2$Li has been consumed, but 50% of the initial **3-Cl** remained. After an additional equivalent of ^{t}BuCH$_2$Li (65 mg, 0.85 mmol) was added and the mixture stirred for 6 h, the solvent was removed and the solid was extracted and washed once with 10 mL of pentane. The pentane was removed under vacuum and replaced with 3 mL of Et$_2$O. Cooling to −78 °C and filtration provided colorless microcrystals (210 mg); an additional crop yielded 83 mg of additional material (293 mg, 39% total). IR (Nujol, cm^{-1}): 3262 (w, NH), 3217 (w, NH), 1235 (w), 1221 (w), 1192 (w), 1180 (w), 1169 (w), 1143 (m), 1096 (s, br), 1087 (s, br), 1012 (m), 986 (w), 933 (m), 855 (s, br), 820 (s, br), 722 (w), 621 (s, br). Anal. Calcd for TaC$_{41}$H$_{94}$N$_3$Si$_3$: C, 55.06; H, 10.59; N, 4.69. Found: C, 54.92; H, 10.53; N, 4.71.

10. (^{t}Bu$_3$SiNH)(^{t}Bu$_3$SiO)MeTa═NSi^{t}Bu$_3$ (5-Me). To a flask containing an intimate mixture of (^{t}Bu$_3$SiNH)Me$_2$Ta═NSi^{t}Bu$_3$ (1, 302 mg, 0.473 mmol) and ^{t}Bu$_3$SiOH (102 mg, 0.473 mmol) was distilled 5 mL of hexanes by vacuum transfer. The solution was stirred for 0.5 h at 25 °C, concentrated to 2–3 mL and cooled to −78 °C. Colorless crystals were collected by filtration (205 mg, 52%). IR (Nujol, cm^{-1}): 3278 (m, NH), 1367 (m), 1167 (m), 1124 (s, br), 1082 (s, br), 1014 (m), 1008 (m, sh), 932 (m), 905 (s, br), 845 (s, br), 817 (s, br), 735 (w), 625 (s, br).

General Kinetics. 1. 1,2-RH-Elimination from 3-R. Solutions of 3-R in the appropriate deuterated solvent were prepared in 2-mL volumetric flasks. Three samples of about 0.3 mL each were transferred to flame-dried, 5-mm NMR tubes sealed to Ŧ 14/20 joints and attached to 180° needle valves. The tubes were freeze–pump–thaw degassed three cycles (77 K) and flame-sealed under vacuum. The three sample tubes were simultaneously heated by immersion in a silicone oil bath with a Tamson immersion circulator. The bath temperature of 182.8 °C was stable to ±0.4 °C. Rates of disappearance of amido NH peaks were monitored in all cases except for the benzene loss from 3-Ph (see text), and the determination of k_H/k_D pertaining to (^{t}Bu$_3$SiNH)$_2$MeTa═NSi^{t}Bu$_3$ (3-Me) vs (^{t}Bu$_3$SiND)$_2$MeTa═NSi^{t}Bu$_3$ (3(ND)$_2$Me). Separate tubes of these complexes were measured in tandem by the disappearance of the methyl resonance. All runs were monitored for 5–6 half-lives. Single transient spectra were used to obtain the most reproducible integrals. Rates and uncertainties were obtained by using weighted ($1/\sigma^2$, where σ was obtained from three simultaneous runs), nonlinear least-squares fitting to the exponential form of the rate expression.

2. Equilibrium of 3-CH$_2$Ph and 3-C$_6$H$_4$Me. A 0.033 M solution of (^{t}Bu$_3$SiNH)$_2$(PhCH$_2$)Ta═NSi^{t}Bu$_3$ (3-CH$_2$Ph) in toluene was thermolyzed at 182.8 (4) °C for 312 h (~3 half-lives of 1,2-elimination). The solvent was removed and a ^{1}H NMR spectrum revealed ~40% 3-CH$_2$Ph and ~60% 3-C$_6$H$_4$Me as determined from the ratio of CH$_2$ to CH$_3$ integrals. The latter was identified as a mixture of para (^{1}H NMR (tentative assignments, C$_6$D$_6$) δ 2.22, CH$_3$; 3.97 (NH)$_2$; 8.10, 8.24, A$_2$B$_2$, J = 6.3 Hz, 4 H) and meta or ortho (^{1}H NMR (tentative assignments, C$_6$D$_6$) δ 2.04, CH$_3$; 5.41 (NH)$_2$; 7.09, ArH, m, 1 H; 8.20 ArH, m, 3 H) isomers, and was treated collectively (see text). Thermolysis for an additional 480 h (~4 half-lives) resulted in little change in the equilibrium (i.e., ~38% 3-CH$_2$Ph and ~62% 3-C$_6$H$_4$Me); hence, the experiment was discontinued.

3. Approach to Equilibrium by 3-Ph and MeH in C$_6$D$_{12}$. A solution of (^{t}Bu$_3$SiNH)$_2$PhTa═NSi^{t}Bu$_3$ (3-Ph) in C$_6$D$_{12}$ was prepared in a 2-mL volumetric flask. Three aliquots of 0.3 mL each were transferred into three flame-dried, thick-walled NMR tubes sealed to Ŧ 14/20 joints and attached to 180° needle valves. The tubes were freeze–pump–thaw degassed three cycles (77 K), and 0.9 atm of methane was introduced into the tubes through a −78 °C trap. The needle valves were closed, the methane was condensed into each tube at 77 K, and the tubes were flame-sealed. The three sample tubes were simultaneously heated by immersion in a silicone oil bath with a Tamson immersion circulator. The bath temperature of 182.8 °C was stable to ±0.4 °C. Rates of disappearance or appearance of amido NH peaks were monitored for (^{t}Bu$_3$SiNH)$_2$PhTa═NSi^{t}Bu$_3$ (3-Ph), (^{t}Bu$_3$SiNH)$_2$MeTa═NSi^{t}Bu$_3$ (3-Me), and [(^{t}Bu$_3$SiNH)$_2$Ta═NSi^{t}Bu$_3$]$_2$(μ_2:η^1,η^1-1,4-C$_6$H$_4$) ((3)$_2$C$_6$H$_4$); (3)$_2$C$_6$H$_4$ was characterized by two singlets of equal integration at δ 7.92 (C$_6$H$_4$) and 5.22 ppm (NH) (the resonances due to the ^{t}Bu groups were coincident with those of 3-Ph and 3-Me). Single transient spectra were used to obtain the most reproducible integrals. The concentration of methane in the solution at room temperature was determined by ^{1}H NMR and observed to remain constant, within experimental error, throughout the experiment. Concentrations of the three tantalum species approached equilibrium, but the slight degradation of samples through prolonged heating hampered efforts to monitor the experiment beyond a certain point. After completion of the experiment, solvent heights and the dimensions of the sample tubes were measured. The tubes were cracked open under vacuum and the volatiles were passed through a series of −78 °C traps into a Toepler pump in order to measure methane volumes. Head gas pressures at 456.0 K were then calculated and the resulting methane concentrations were inferred from the data of Reamer, Sage, and Lacey.[81]

Table V. Atomic Coordinates (×10^4) and Equivalent Isotropic Displacement Coefficients (U's, Å^2 × 10^3)

	x	y	z	U(eq)
Ta	202 (1)	325 (1)	1675 (1)	35 (1)
C1	162 (20)	−1143 (13)	2090 (8)	70 (8)
N3	−1084 (11)	566 (10)	2355 (6)	50 (5)
C2	−1989 (17)	25 (16)	2384 (9)	73 (9)
C3	−2742 (16)	84 (18)	2808 (10)	70 (9)
C4	−2530 (22)	735 (21)	3208 (9)	90 (11)
C5	−1583 (17)	1287 (17)	3178 (8)	63 (8)
C6	−905 (17)	1215 (16)	2763 (9)	64 (8)
N4	−406 (14)	1947 (10)	1561 (6)	58 (6)
C7	211 (22)	2635 (15)	1456 (9)	78 (8)
C8	72 (28)	3567 (22)	1295 (12)	107 (14)
C9	−1023 (35)	3789 (19)	1210 (12)	108 (16)
C10	−1769 (30)	3137 (25)	1310 (14)	125 (16)
C11′	−1484 (19)	2195 (17)	1519 (10)	78 (9)
N1	−236 (13)	−69 (10)	1013 (5)	54 (5)
Si1	−564 (4)	−425 (5)	375 (2)	54 (2)
C11	−500 (26)	−1860 (18)	352 (10)	93 (11)
C111	467 (41)	−2229 (17)	623 (14)	228 (31)
C112	−577 (28)	−2326 (19)	−210 (11)	138 (16)
C113	−1421 (36)	−2358 (24)	679 (13)	211 (26)
C12	−2049 (19)	53 (29)	267 (11)	114 (16)
C121	−2043 (33)	1216 (26)	171 (16)	192 (25)
C122	−2769 (21)	−152 (31)	738 (10)	145 (18)
C123	−2612 (22)	−351 (32)	−231 (10)	160 (19)
C13	447 (20)	157 (21)	−105 (8)	90 (10)
C131	667 (28)	1226 (19)	39 (12)	139 (16)
C132	104 (25)	157 (20)	−713 (8)	129 (14)
C133	1561 (22)	−406 (27)	−86 (17)	193 (23)
N2	1665 (11)	594 (9)	1741 (6)	44 (5)
Si2	3051 (4)	630 (3)	1884 (2)	46 (2)
C21	3776 (17)	1479 (19)	1377 (10)	70 (9)
C211	4965 (18)	1785 (21)	1540 (10)	103 (12)
C212	3134 (21)	2395 (20)	1237 (11)	99 (12)
C213	3890 (22)	909 (25)	857 (11)	125 (15)
C22	3162 (19)	1173 (15)	2613 (9)	65 (8)
C221	4325 (17)	1076 (18)	2860 (10)	82 (10)
C222	2326 (20)	728 (19)	2991 (10)	84 (10)
C223	2952 (24)	2297 (18)	2604 (11)	111 (13)
C23	3618 (19)	−731 (16)	1888 (10)	72 (9)
C231	3223 (22)	−1324 (16)	2360 (9)	83 (10)
C232	4917 (16)	−787 (19)	1849 (10)	88 (10)
C233	3140 (18)	−1310 (16)	1389 (10)	77 (9)

[a] Equivalent isotropic U is defined as one-third of the trace of the orthogonalized $\mathbf{U}_{ij}$ tensor.

A Runge–Kutta simulation[75] was performed in order to fit the data obtained in the approach to equilibrium experiment. Six differential equations were employed in the simulation, representing the equilibria shown in eqs 20–22 (Scheme II). Rate constants k_1, k_2, and k_3 were

$$\underset{\mathbf{3\text{-}Ph}}{({}^t\mathrm{Bu_3SiNH})_2\mathrm{PhTa{=}NSi}{}^t\mathrm{Bu_3}} \underset{k_{-1}}{\overset{k_1}{\rightleftharpoons}} \underset{\mathbf{4}}{({}^t\mathrm{Bu_3SiNH})\mathrm{Ta}({=}\mathrm{NSi}{}^t\mathrm{Bu})_2} + \mathrm{PhH} \quad (20)$$

$$\underset{\mathbf{3\text{-}Me}}{({}^t\mathrm{Bu_3SiNH})_2\mathrm{MeTa{=}NSi}{}^t\mathrm{Bu_3}} \underset{k_{-2}}{\overset{k_2}{\rightleftharpoons}} \mathbf{4} + \mathrm{MeH} \quad (21)$$

$$\underset{(\mathbf{3})_2\mathrm{C_6H_4}}{[({}^t\mathrm{Bu_3SiNH})_2\mathrm{Ta{=}NSi}{}^t\mathrm{Bu_3}]_2(\mu_2{:}\eta^1,\eta^1\text{-}1,4\text{-}\mathrm{C_6H_4})} \underset{k_{-3}}{\overset{k_3}{\rightleftharpoons}} \mathbf{4} + \mathbf{3\text{-}Ph} \quad (22)$$

varied in order to fit the experimental curves as closely as possible, while those corresponding to trapping of 4 (k_{-1}, k_{-2}, and k_{-3}) were set sufficiently (and necessarily) faster and varied accordingly. While the values of k_1 and k_2 were not constrained to the values determined from the benzene-d_6 thermolyses of 3-Ph and 3-Me in C$_6$D$_6$, the rate constants obtained from the fit are very similar (Table III). The concentrations used to calculate the free energy values were obtained from the Runga–Kutta simulation of the approach to equilibrium (eqs 20–22), and are referenced to a 1 M standard state: for 3-Ph + MeH ⇌ 3-Me + PhH, $K_{eq} = (k_1k_{-2})/(k_{-1}k_2)$ = [3-Me][PhH]/[3-Ph][MeH] = 0.513, ΔG(456 K) = 0.60; for 2 3-Ph ⇌ (3)$_2$C$_6$H$_4$ + PhH, $K_{eq} = (k_1k_{-3})/(k_{-1}k_3)$ = [(3)$_2$C$_6$H$_4$][PhH]/[3-Ph]^2 = 0.259, ΔG(456 K) = 1.22; for 3-Me + 3-Ph ⇌ (3)$_2$C$_6$H$_4$ + MeH, $K_{eq} = (k_2k_{-3})/(k_{-2}k_3)$ = [(3)$_2$C$_6$H$_4$][MeH]/[3-Ph][3-Me] = 0.506, ΔG(456 K) = 0.62.

Single-Crystal X-ray Diffraction Analysis of (py)$_2$MeTa(=NSi^{t}Bu$_3$)$_2$ (2(py)$_2$). A flat, amber needle (0.1 × 0.3 × 0.3 mm) of (py)$_2$MeTa(=NSi^{t}Bu)$_2$ (**2**(py)$_2$), obtained from benzene solution, was sealed in a capillary. Preliminary X-ray diffraction photographs revealed orthorhombic symmetry. Precise lattice constants, determined from a least-squares fit of 15 diffractometer-measured 2θ values at 25 °C, were a = 12.134 (2) Å, b = 13.421 (2) Å, and c = 24.865 (4) Å. The cell volume was 4049.3 (11) Å^3, with a calculated density of 1.281 g/cm, where Z = 4. The space group was determined to be $P2_12_12_1$, and the asymmetric unit consisted of $C_{35}H_{67}N_4Si_2Ta$. All unique diffraction maxima ($+h,+k,+l$) with $2\theta < 50$ were measured on a Syntex P2$_1$ automated diffractometer, by a variable-speed, 2θ–θ scan (1.50–29.30°/min) with graphite-monochromated Mo Kα radiation (λ = 0.710 70 Å) at 25 °C. After correction for Lorentz, polarization, and background effects, 3257 (88.9%) of the unique data (3967) were judged observed ($|F_o| > 3\sigma|F_o|$).[89] All heavy atoms were located using direct methods (SHELXTL PLUS), and all non-hydrogen atoms (Table V) were revealed by successive Fourier syntheses. Full-matrix, least-squares refinements (minimization of $\sum w(F_o - F_c)^2$, where w is based on counting statistics modified by an ignorance factor ($w^{-1} = \sigma^2(F) + 0.0010F^2$)), with anisotropic heavy atoms and all hydrogens included at calculated positions (Riding model, fixed isotropic U), converted to R = 8.81%. A semiempirical absorption correction[90] was applied, and the minimum and maximum absorption corrections were 0.3645 and 1.0000. A final difference Fourier map revealed no peaks greater than 2.76 e/Å^3. For 3257 observed reflections, the final residuals were R = 6.20% and R_w = 6.64%, with GOF = 1.35.[91]

Acknowledgment. Primary support from the National Science Foundation (Grant CHE-8714146) is gratefully acknowledged as are contributions from the Air Force Office of Scientific Research (Grant AFOSR-87-0103) and Cornell University. We thank Prof. Barry K. Carpenter and Prof. Frank Feher for helpful discussions, and Dr. Gregory D. Van Duyne for aid in the crystallographic study. Support for the Cornell NMR Facility from the NIH and NSF Instrumentation Programs is acknowledged.

Supplementary Material Available: X-ray structural information pertaining to (py)$_2$MeTa(=NSi^{t}Bu$_3$)$_2$ (**2**(py)$_2$), including listings of crystal data encompassing data collection and solution/refinement, atomic coordinates, isotropic and anisotropic temperature factors, hydrogen atom coordinates, bond lengths, and bond angles (9 pages). Ordering information is given on any current masthead page.

---

(89) Cromer, D. T.; Mann, J. B. *Acta Crystallogr., Sect. A* **1968**, *A24*, 321–324.

(90) Walker, N.; Stuart, D. *Acta Crystallogr., Sect. A* **1983**, *139*, 158–166.

(91) $R = \sum||F_o| - |F_c||/(\sum|F_o|)$; $R_w = \{\sum w(|F_o| - |F_c|)^2/\sum w(|F_o|)^2\}^{1/2}$; GOF = $\{\sum[\text{weight} \times (|F_o| - |F_c|)^2]\}/(M - N)$ where M = number of observations and N = number of parameters; 3257 (88.9%) reflections with $|F_o| \geq 3\sigma(F_o)$.